Phase Diagram of the $\nu = 5/2$ Fractional Quantum Hall Effect: Effects of Landau-Level Mixing and Nonzero Width

Kiryl Pakrouski,[1] Michael R. Peterson,[2] Thierry Jolicoeur,[3] Vito W. Scarola,[4] Chetan Nayak,[5,6] and Matthias Troyer[1]

[1]*Theoretische Physik, ETH Zurich, 8093 Zurich, Switzerland*
[2]*Department of Physics and Astronomy, California State University Long Beach,
Long Beach, California 90840, USA*
[3]*Laboratoire de Physique Théorique et Modèles Statistiques, CNRS and Université Paris-Sud,
91405 Orsay, France*
[4]*Department of Physics, Virginia Tech, Blacksburg, Virginia 24061, USA*
[5]*Department of Physics, University of California, Santa Barbara, California 93106, USA*
[6]*Microsoft Research, Station Q, Elings Hall, University of California, Santa Barbara, California 93106, USA*
(Received 21 November 2014; published 2 April 2015)

Interesting non-Abelian states, e.g., the Moore-Read Pfaffian and the anti-Pfaffian, offer candidate descriptions of the $\nu = 5/2$ fractional quantum Hall state. But, the significant controversy surrounding the nature of the $\nu = 5/2$ state has been hampered by the fact that the competition between these and other states is affected by small parameter changes. To study the phase diagram of the $\nu = 5/2$ state, we numerically diagonalize a comprehensive effective Hamiltonian describing the fractional quantum Hall effect of electrons under realistic conditions in GaAs semiconductors. The effective Hamiltonian takes Landau-level mixing into account to lowest order perturbatively in κ, the ratio of the Coulomb energy scale to the cyclotron gap. We also incorporate the nonzero width w of the quantum-well and subband mixing. We find the ground state in both the torus and spherical geometries as a function of κ and w. To sort out the nontrivial competition between candidate ground states, we analyze the following four criteria: its overlap with trial wave functions, the magnitude of energy gaps, the sign of the expectation value of an order parameter for particle-hole symmetry breaking, and the entanglement spectrum. We conclude that the ground state is in the universality class of the Moore-Read Pfaffian state, rather than the anti-Pfaffian, for $\kappa < \kappa_c(w)$, where $\kappa_c(w)$ is a w-dependent critical value $0.6 \lesssim \kappa_c(w) \lesssim 1$. We observe that both Landau-level mixing and nonzero width suppress the excitation gap, but Landau-level mixing has a larger effect in this regard. Our findings have important implications for the identification of non-Abelian fractional quantum Hall states.

I. INTRODUCTION

The $\nu = 5/2$ fractional quantum Hall state is well established: It has a robust energy gap and has been observed in a large number of different GaAs samples [1–23], yet its underlying quantum order remains mysterious. Although there is strong evidence that the ground state is spin polarized [24] with a fractional quasiparticle effective charge of $e/4$ [11,13,25,26], there are some experiments that remain difficult to interpret in this light [27,28]. Perhaps the most interesting hypothesized property of this state—non-Abelian quasiparticle braiding [29–36]—is controversial. There are experiments consistent with non-Abelian quasiparticles [25,37–39] but also some experiments that are not [40,41].

Theoretical guidance can play an important role in identifying the state. Exact-diagonalization [42–49] and density-matrix renormalization-group [50,51] studies of simplified model Hamiltonians show that non-Abelian states, such as the Moore-Read (MR) Pfaffian state [52] and the anti-Pfaffian (aPf) state [53,54], are viable ground states, but transitions to other ground states can occur as a result of small changes in Hamiltonian parameters [43–45,48]. Since the details of the Hamiltonian matter (unlike in the case of states in the lowest Landau level, such as the $\nu = 1/3$ state), it is important to analyze Hamiltonians that model realistic experimentally relevant systems and include effects such as Landau-level mixing and the finite width of the quantum well. Moreover, only a particle-hole symmetry-breaking effect, such as Landau-level mixing, can split the degeneracy between the MR Pfaffian and aPf states [55,56].

The exact-diagonalization study of Ref. [48] found the ground state for the half filled $N = 1$ Landau level for

systems with up to $N_\Phi = 2N_e - S = 33$ magnetic flux quanta in the spherical geometry using an effective Hamiltonian [57] that included Landau-level mixing with virtual excitations to the $N = 0$ and $N > 1$ Landau levels integrated out perturbatively to lowest order in

$$\kappa = \left(\frac{e^2}{\epsilon \ell_0}\right)/\hbar \omega_c \propto 1/\sqrt{B}. \tag{1}$$

($\ell_0 = \sqrt{\hbar c/eB}$ is the magnetic length, ϵ is the dielectric constant of the host semiconductor, $\omega_c = eB/mc$ is the cyclotron frequency, and S is a topological quantum number called the shift [58].) The ground state at the MR Pfaffian shift of $S = 3$ was found to have larger overlap with the MR Pfaffian wave function than the ground state at the aPf shift of $S = -1$ had with the aPf wave function, indicating, naively, that the ground state was in the MR Pfaffian universality class. Two caveats are that (1) Ref. [48] used two-body pseudopotentials [57] with a subtle normal-ordering error that was corrected later [59–61] and (2) these results only took account of the finite width of the quantum well via a scaling of the pseudopotentials. Meanwhile, an exact-diagonalization study [47] of a truncated Hamiltonian for a few Landau levels found larger overlap with the aPf wave function on the torus. (Similar ideas were used in Ref. [62].) Reference [47] used a truncated Hamiltonian approximation in hopes that it would capture the correct physics at intermediate values of κ, even though it is uncontrolled; i.e., it is not exact in any limit, unlike the Hamiltonians of Refs. [57,59–61], which are exact in the $\kappa \to 0$ limit. Moreover, the overlap between a ground state and a trial wave function may reflect short-distance non-universal details of that particular trial wave function, rather than its universality class. Indeed, such an overlap vanishes in the thermodynamic limit.

In this paper, we solve an effective Hamiltonian that incorporates both Landau-level mixing and finite quantum-well width. We then analyze the resulting ground states and low-lying excited states by several criteria. We begin by describing our effective Hamiltonian and providing a qualitative picture in Secs. II and III. In Sec. IV, we compute the overlaps in the spherical geometry between the ground states at $S = 3$ and $S = -1$ with, respectively, the MR Pfaffian and the aPf wave functions, and on the torus using the hexagonal unit cell where the MR Pfaffian and aPf occur at the same flux and are orthogonal for an odd number of electrons. We corroborate our overlap findings in Sec. V by calculating the entanglement spectrum. In Sec. VI, we compare the energy gaps in the spherical geometry at $S = 3$ and $S = -1$ and provide estimates of the excitation gaps in the thermodynamic limit that take into account Landau-level mixing and finite width. In Sec. VII, we introduce an operator that is odd under a particle-hole transformation and, therefore, can be used as an order parameter distinguishing between the MR Pfaffian

and aPf states. We compute this order parameter in the ground state of our Hamiltonian on the torus and sphere. According to all of these criteria, our central finding is that there is a $\kappa_c(w)$ such that the ground state for $0 < \kappa < \kappa_c(w)$ is in the universality class of the MR Pfaffian. We find that $\kappa_c(0) \approx 0.6$, monotonically increasing to $\kappa_c(4\ell_0) \approx 1$.

A phase transition occurs at $\kappa = \kappa_c(w)$, identified by the collapse of both the energy gap and the overlap with the MR Pfaffian wave function, as well as a sharp peak in the bipartite entanglement entropy. For $w < 1.5\ell_0$, there appears to be a second phase transition at slightly larger κ. The intermediate phase between the two transitions may be a different fractional quantum Hall state, such as the aPf or a strong pairing phase [63], but the gap is too small for us to say anything definitive at these system sizes. We culminate our findings in a phase diagram.

II. EFFECTIVE HAMILTONIAN

We diagonalize an effective Hamiltonian for spin-polarized electrons confined to the $N = 1$ Landau level that incorporates the effects of Landau-level mixing and finite width. Finite width causes a "softening" of the Coulomb interaction at short distances, and the Coulomb interaction can now cause virtual electron excitations to higher subbands of the quantum well in addition to higher Landau levels. Hence, we take Landau-level and subband mixing into account perturbatively to lowest order in κ through the terms that are generated by virtual excitations of electrons to the $N = 2, 3, \ldots$ Landau levels and higher quantum-well subbands or of holes to the $N = 0$ Landau level. As noted in Ref. [59], virtual excitations into all unoccupied Landau levels are taken into account in this perturbative scheme producing a controlled model that is exact in the $\kappa \to 0$ limit. Our model is in contrast to Landau-level-mixing models that work in an expanded, yet truncated, Hilbert space that are uncontrolled and not exact in any limit [47,64,65]. Our effective Hamiltonian has the form

$$H(w/\ell_0, \kappa, N = 1) = \sum_m V_m^{(2)}(w/\ell_0, \kappa) \sum_{i<j} \hat{P}_{ij}(m)$$
$$+ \sum_m V_m^{(3)}(w/\ell_0, \kappa) \sum_{i<j<k} \hat{P}_{ijk}(m), \tag{2}$$

where $\hat{P}_{ij}(m)$ and $\hat{P}_{ijk}(m)$ are projection operators that project, respectively, the pair i, j or triplet i, j, k of electrons onto states of relative angular momentum m. $V_m^{(2)}(w/\ell_0, \kappa)$ and $V_m^{(3)}(w/\ell_0, \kappa)$ are the two- and three-body effective pseudopotentials [66,67], with dependence on the well width w/ℓ_0 and Landau-level-mixing parameter κ denoted explicitly. In addition to the numerical renormalization of the two-body interaction, particle-hole symmetry-breaking three-body terms are produced [68]. For our calculations,

we use the corrections to the two-body pseudopotentials and the three-body pseudopotentials that can be found in Tables I and II and Figs. 4–8 of Ref. [59] (see also Ref. [69]). We only take into account the lowest $V_m^{(3)}$ for $m \leq 8$. Our results indicate that including higher three-body pseudopotentials has no effect on our conclusions, which is discussed in more detail in Appendix D.

In our calculations on the sphere, N_e electrons are placed on a spherical surface of radius $\sqrt{N_\Phi/2}$ with a radial magnetic field produced by a magnetic monopole of strength $N_\Phi/2$ at the center. ($N_\Phi/2$ is an integer or half-integer by Dirac's quantization condition.) The total angular momentum L is a good quantum number, and any fractional quantum Hall state will be uniform and incompressible with $L = 0$ [66,70]. For half filling, we have $N_\Phi = 2N_e - S$; the filling factor in the $N = 1$ Landau level is given by $\nu = \lim_{N_e \to \infty} N_e/N_\Phi$. As noted above, the MR Pfaffian has $S = 3$ while the aPf has $S = -1$, which can be seen by particle-hole transforming the MR Pfaffian.

We model finite width using both an infinite square well and Gaussian single-particle wave functions in the z direction, perpendicular to the two-dimensional electron gas. We find that results for these two models are very similar and can be converted one into the other, as we discuss further in Appendix A. Thus, we show only results for an infinite square well.

We note that while we work in the spherical geometry, we utilize planar geometry pseudopotentials. It has been argued that planar geometry pseudopotentials more accurately represent the thermodynamic limit [45]. Furthermore, we extrapolate several of our results to the thermodynamic limit and find that the choice of pseudopotentials is not crucial (see Appendix D).

We also consider the torus geometry. The torus is a two-dimensional plane with periodic boundary conditions with pseudomomentum **K** in a Brillouin zone that can be either rectangular or hexagonal. On the torus, there is no shift, and $N_\Phi = 2N_e$, which makes a direct comparison between MR Pfaffian and aPf states more straightforward.

III. QUALITATIVE PICTURE

There is very strong evidence that the ground state of Eq. (2) is in the MR or aPf universality class for $\kappa = 0$ and that finite thickness increases the stability of this ground state [42–45]. This conclusion is true using the torus or spherical geometry. A remaining question, and the one we answer here, is what happens under the influence of a particle-hole symmetry-breaking effect like Landau-level mixing; i.e., is the ground state in the MR or aPf universality class or neither universality class?

On the torus, at $\kappa = 0$, the ground state is doubly degenerate in the thermodynamic limit (over and above the sixfold topological degeneracy on the torus). One of these states is in the MR Pfaffian universality class, and the

other is in the aPf universality class; their degeneracy is guaranteed by particle-hole symmetry. On the sphere, the former occurs at $S = 3$ and the latter at $S = -1$. As κ is increased, the two-body terms are modified and three-body terms are generated. The former cannot break the symmetry between the MR and aPf states since they preserve particle-hole symmetry.

To understand the effect of the latter qualitatively, we consider their effect to lowest order in perturbation theory; i.e., we compute the expectation value of $H_{3body} = \sum_m V_m^{(3)}(w/\ell_0, \kappa) \sum_{i<j<k} \hat{P}_{ijk}(m)$ in the two ground states on the sphere. As may be seen from Fig. 1, the energy of the $S = 3$ state (MR) is lowered more than that of the $S = -1$ state (aPf).

The preceding calculation is done at $N_\Phi = 33$. To check whether this conclusion is likely to hold in the thermodynamic limit, we repeat it for different system sizes and consider the extrapolation to $N_e = \infty$. In Fig. 2, we plot the expectation value per particle of the three-body terms of $H(w/\ell_0 = 0, \kappa = 0.1, 1)$ given in Eq. (2) evaluated in the Coulomb ground state for systems with $N_\Phi = 13$ to $N_\Phi = 37$. A linear fit in the inverse number of particles or holes provides an estimate for the thermodynamic limit. We observe that the energy at $S = 3$ is lowered more than at $S = -1$ for all available system sizes as well as in the thermodynamic limit. The result in the thermodynamic limit is in agreement with our conclusions drawn in the previous paragraph and in Fig. 1. Thus, from this result, we expect the MR state to be the ground state for small κ. We verify this expectation by exact diagonalization in the sections that follow.

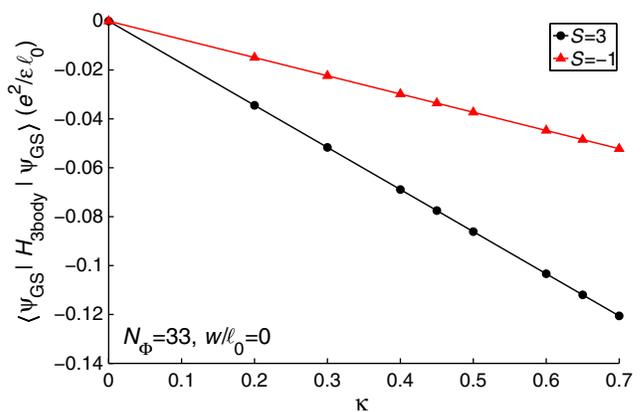The manner in which the three-body terms favor the MR state is subtle. The lowest angular-momentum term

FIG. 1. Expectation value of the three-body terms in the Hamiltonian $\langle \Psi_{GS}|H_{3body}|\Psi_{GS}\rangle$ in the $S = 3$ (MR) and $S = -1$ (aPf) ground states obtained at $\kappa = 0$ and $w/\ell_0 = 0$ in the system with $N_\Phi = 33$ in the spherical geometry. Here, H_{3body} is the second term in Eq. (2) and introduces κ dependence. H_{3body} is the lowest-order perturbative contribution to the energies of these states. The energy of the $S = 3$ (MR) state is lowered more.

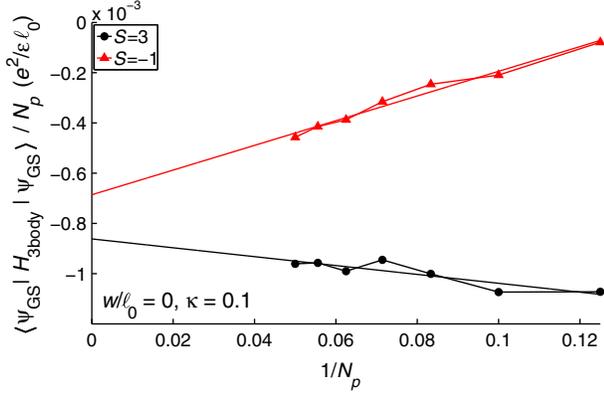FIG. 2. The expectation value of the three-body terms in the Hamiltonian $\langle \Psi_{GS}|H_{3body}|\Psi_{GS}\rangle$ per particle at various system sizes. $\langle \Psi_{GS}|H_{3body}|\Psi_{GS}\rangle$ is the leading contribution to the energy difference between these states computed perturbatively in κ. N_p is the number of electrons for $S = 3$ and number of holes for $S = -1$. The energy difference between the extrapolated values is $0.00018 e^2/\epsilon\ell_0 = 0.12\kappa|V_3^{(3)}|$.

$V_3^{(3)}(w/\ell_0, \kappa)$ has a vanishing expectation value in the MR trial wave function and a small but negative expectation value in the aPf trial wave function, and, therefore, one might expect the aPf state to have lower energy if $V_3^{(3)}(w/\ell_0, \kappa)$ dominates over higher angular momenta. However, as may be seen from the top panel of Fig. 3, the energy contributions of the $V_m^{(3)}(w/\ell_0, \kappa)$ for $m = 5$ and 6 are generally larger and will dominate. (We have chosen $w/\ell_0 = 0$ and $\kappa = 0.2$ for illustrative purposes.) Of course, the MR wave function has a vanishing expectation value of $V_3^{(3)}(w/\ell_0, \kappa)$ since this operator completely annihilates the wave function; i.e., the MR wave function is the zero-energy ground state of $\sum_{i<j<k} \hat{P}_{ijk}(3)$ from which $V_3^{(3)}(w/\ell_0, \kappa)$ is constructed. The aPf wave function has a nearly zero expectation value of $V_3^{(3)}(w/\ell_0, \kappa)$ because at $S = -1$ we can particle-hole transform $V_3^{(3)}(w/\ell_0, \kappa)$ to give a three-body operator that exactly annihilates the aPf wave function but also produces two-, one-, and zero-body terms. Thus, $V_m^{(3)}(w/\ell_0, \kappa)$ for $m > 3$ terms will largely determine which state has lower energy. Moreover, the above expectation remains when we use the actual Coulomb ground state, again for $w/\ell_0 = 0$ and $\kappa = 0.2$, rather than the trial wave functions. Then, we find that the energy difference due to $V_3^{(3)}(w/\ell_0, \kappa)$ becomes negligible and the relative importance of the higher angular momenta is enhanced, as may be seen in the bottom panel of Fig. 3. Hence, the effect of the three-body terms due to Landau-level mixing and finite width cannot be simply modeled by considering only the lowest three-body relative angular-momentum ($m = 3$) term—the need for higher order angular momenta is similar to how the effect of finite width alone cannot be completely understood by simply
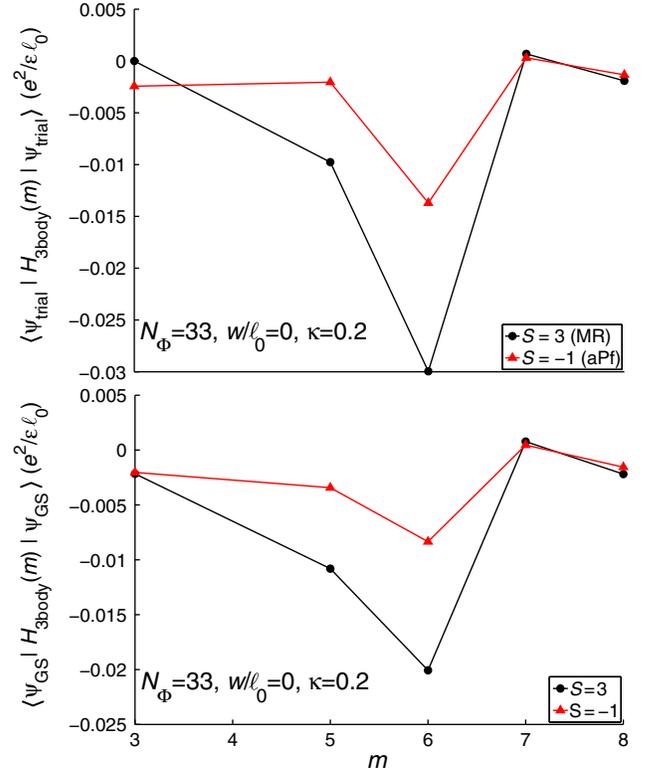

FIG. 3. Top panel: Expectation value of the three-body terms in the MR and aPf trial wave functions as a function of angular momentum m, i.e., $\langle \Psi_{trial}|H_{3body}(m)|\Psi_{trial}\rangle$ where $H_{3body}(m) = V_m^{(3)}(w/\ell_0, \kappa)\sum_{i<j<k}\hat{P}_{ijk}(m)$, and $\Psi_{trial} = \Psi_{MR}$ or Ψ_{aPf}. Bottom panel: Expectation value of the three-body terms for the $S = 3$ and $S = -1$ ideal Coulomb ground states as a function of angular momentum m.

looking at the ratio of the $m = 1$ and $m = 3$ Haldane pseudopotentials [45].

IV. WAVE-FUNCTION OVERLAP

According to the argument of the previous section, the ground state is in the MR universality class for small κ. We now corroborate the arguments of the previous section using wave-function overlap.

The MR wave function takes the following form on the sphere:

$$\Psi_{MR} = \text{Pf}\left(\frac{1}{u_i v_j - v_i u_j}\right)\prod_{i>j}(u_i v_j - v_i u_j)^2, \qquad (3)$$

where $(u_i, v_i) = (e^{-i\phi_i/2}\cos\theta_i, e^{i\phi_i/2}\sin\theta_i)$ are the spherical coordinates of the ith particle. Here, Pf denotes the Pfaffian, i.e., the square root of the determinant of an antisymmetric matrix. On the torus, this wave function takes the form

$$\Psi_{\mathrm{MR}} = \mathrm{Pf}\left(\frac{\vartheta_a(z_i - z_j)}{\vartheta_1(z_i - z_j)}\right)\prod_{i>j}[\vartheta_1(z_i - z_j)]^2\Phi_{\mathrm{c.m.}}\left(\sum_i z_i\right).$$

$$(4)$$

Here, $\vartheta_1(z)$ and $\vartheta_a(z)$, $a = 2, 3, 4$, are the Jacobi theta functions and $\Phi_{\mathrm{c.m.}}(\sum_i z_i)$ is the center-of-mass wave function. z_i is a complex planar coordinate of the ith particle. The aPf wave functions on the sphere and torus are obtained by taking the particle-hole conjugates of these wave functions.

Figure 4 shows the numerical wave-function overlaps between the ground state at $S = 3$ and $S = -1$ for $N_\Phi = 33$ and, respectively, the MR and aPf wave functions on the sphere as a function of κ for $w/\ell_0 = 0, 1, 2$, and 3. An overlap of unity or 0 means the exact ground state of Eq. (2) is either identical to or completely different from the trial MR or aPf wave function. We remind readers that an overlap is not a universal quantity of a ground state that can be extrapolated to the thermodynamic limit since, unless it is unity for all N_e, it will vanish as the number of particles goes to infinity. The overlap between the ground state of Eq. (2) and both the MR and aPf wave functions is reasonably large for small κ and drops dramatically at larger κ, falling to 0 somewhere in the range 0.7–1.0, with larger κ occurring for larger widths. Importantly, the overlap with the MR state is consistently larger. Although not shown here, smaller system results are consistent with the $N_\Phi = 33$ results. The larger overlap is an indication that the ground state is likely to be in the same universality class as the MR state for small κ. But, as we cautioned above, it is possible that the aPf's smaller overlaps are merely expressing the fact that
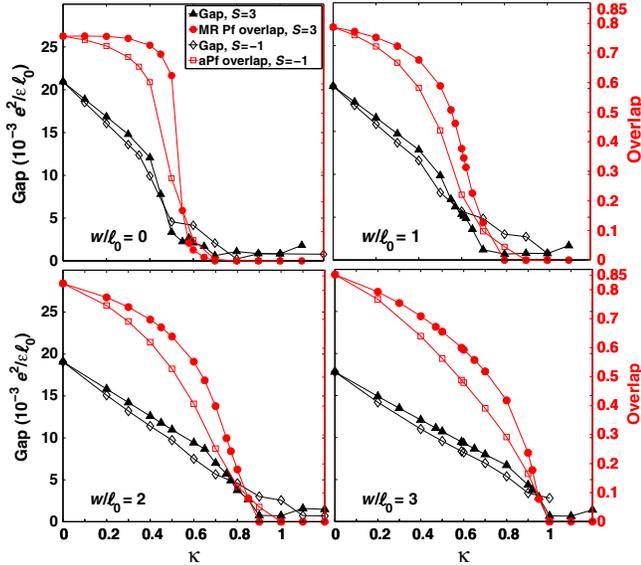
nonuniversal short-distance physics is not well captured by this wave function.

On the torus, the MR and aPf states occur at precisely the same flux. With a rectangular unit cell, the MR and aPf states are threefold degenerate (after factoring out the twofold center-of-mass degeneracy) with each zero-energy state existing at $\mathbf{K} = (0, N_0/2)$, $(N_0/2, 0)$, and $(N_0/2, N_0/2)$, where N_0 is the greatest common divisor of N_e and N_Φ. K_x and K_y are in units of $2\pi\hbar/a$ and $2\pi\hbar/b$, where b/a is the aspect ratio of the rectangular unit cell. Generically, in this geometry, the MR and aPf are not orthogonal, rendering ambiguous the use of overlaps. However, in the hexagonal unit cell containing an odd number of electrons, the MR and aPf states are orthogonal and both have $\mathbf{K} = (0, 0)$. At $\kappa = 0$, the Coulomb ground state is a doublet at $\mathbf{K} = (0, 0)$ (provided $N_e \neq 6n + 1$) and we find that for nonzero κ, this doublet is split in such a way that each member has a nonzero overlap with either the MR or aPf state, as described by Papić *et al.* [64]. The lowest-lying state has nonzero overlap only with the MR state.

The top panel of Fig. 5 shows the overlap between the MR state and the ground state for the hexagonal unit cell as a function of κ and w/ℓ_0 for $N_e = 15$. The overlap is relatively large, dropping to 0 at a critical κ in the range 0.6–1, with larger values occurring for larger widths. Meanwhile, on the torus, the first excited state has a similarly large overlap with the aPf wave function, essentially mirroring the overlap between the ground state and the MR wave function. The overall shape of the overlap is very similar to that on the sphere, shown in the bottom panel of Fig. 5, further corroborating previous results, and, as we show below, these conclusions are supported by criteria that do not depend on any particular trial wave functions.

Our results for $S = -1$ on the sphere and for the first excited state on the torus are a bit surprising. If the ground
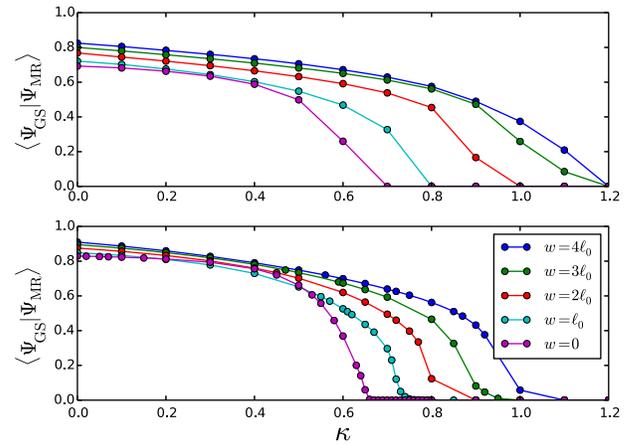

FIG. 4. Energy gap (energy difference between the two lowest states) and model wave-function overlap ($N_\Phi = 33$ system) at the MR Pfaffian ($N_e = 18$) and aPf ($N_e = 16$) shifts. Note that for small κ, both the gap and overlaps are higher for the MR Pfaffian than they are for the aPf.

FIG. 5. The overlap between the ground state and the MR wave function as a function of κ, for $w/\ell_0 = 0, 1, 2, 3$, and 4. $w/\ell_0 = 0$ is the leftmost curve, and $w/\ell_0 = 4$ is the rightmost. The top panel is on the torus for $N_e = 15$ and the hexagonal unit cell, with the bottom panel for the sphere with $N_\phi = 29$ with $S = 3$ ($N_e = 16$).

state at $S = 3$ is firmly in the MR universality class, then the ground state at $S = -1$ should have eight quasiholes on the $S = 3$ ground state. Instead, it has high overlap with the aPf state. Similarly, the first excited state on the torus should look like an exciton on the MR ground state, but, instead, it has high overlap with the aPf ground state. If the ground state is in the universality class of the MR state, then the energy gap to a state with high overlap with the aPf should be extensive in system size. What we observe can thus only happen in small systems. For larger system sizes, the $S = -1$ ground state on the sphere and the first excited state on the torus must look, respectively, like the $S = 3$ ground state on the sphere or the torus with excitations on top. It is possible, in principle, to correctly identify the ground state in the thermodynamic limit without correctly identifying the precise ordering of excited states. The latter can change without the gap closing. That appears to be what is occurring in our case. The finite-size extrapolation shown in Figs. 2 and 17 shows that the corrections that we include favor the MR Pfaffian ground state. (Similarly, the exciton gap shows scaling with system size.) However, the first excited state does not scale as simply with system size. The lack of simple scaling is presumably an indication that there are level crossings among the excited states that occur on the way to the thermodynamic limit, and these prevent us from correctly identifying the precise ordering of the excited states. Such a scenario must occur in the present case since the anti-Pfaffian state cannot be the first excited state at large N_e. While we have not shown that a change in the order of the excited states for large system sizes occurs in our model, we see no evidence for gap closure as N_e is increased, supporting our identification of the correct ground state.

V. ENTANGLEMENT SPECTRUM

We have called the $S = 3$ and $S = -1$ ground states the MR state and the aPf state, respectively, due to their large overlaps with the corresponding trial wave functions [Eq. (3), and its particle-hole conjugate]. However, the overlap with trial wave functions is not universal and vanishes in the thermodynamic limit. Therefore, we now identify these states by a universal criterion, the entanglement spectrum.

In the spherical geometry, we divide the system in two pieces A and B [71–75] and obtain the reduced density matrix for one-half by tracing out the degrees of freedom of the remaining half. The eigenvalues ρ_n of the density matrix are interpreted as energies $\rho_n \equiv e^{-\xi_n/2}$ [76]. If we make a cut in orbital space, then the entanglement spectrum for a state in the MR universality class should have negative slope for the entanglement energies as a function of the z component of the angular momentum L_z^A in sector A, for example, as discussed in Ref. [76].

A state in the MR Pfaffian universality class displays the following structure in the entanglement spectrum: The spectrum is essentially divided into two pieces by a "gap"

with the low-lying states corresponding to the conformal field theory describing the MR edge states. Starting from the "root" configuration of the MR states, one can define $\Delta L_z^A = (L_z^A)_{\text{root}} - L_z^A$, where $(L_z^A)_{\text{root}}$ is the z component of angular momentum of the root configuration; see Ref. [76]. The slope of the "energy" spectra, i.e., whether ΔL_z^A is positive or negative as a function of L_z^A, expresses the chirality of the edge modes of the conformal field theory. In our convention, a state in the MR universality class has an entanglement spectrum with a negative slope. Thus, the entanglement spectrum for a state in the aPf universality class has a positive slope corresponding to edge modes with opposite chirality.

Figure 6 shows that the entanglement spectrum at $S = 3$ for $\kappa = 0.1$ and $w/\ell_0 = 1$ has negative slope, similar to that of the entanglement spectrum for the MR trial wave function; see Eq. (3). Meanwhile, the entanglement spectrum at $S = -1$ has positive slope, similar to that of the aPf trial wave function [the particle-hole conjugate of Eq. (3)]. We therefore find that both the entanglement spectrum and overlaps allow us to identify the $S = 3$ and $S = -1$ ground states as the MR state and the aPf state, respectively. The phase transition at $\kappa \approx 0.6$–1.0 is also observed in the entanglement spectra, as shown in Fig. 7 and discussed further in Sec. VIII. As κ increases, the structure of the low-lying states first changes chirality and then changes completely and no longer resembles the MR or aPf entanglement spectra.

We adopt the definition of the "topological gap" for the Pfaffian-like phase introduced in Ref. [76] with $\Delta L_z^A = 0$, thus defining it as the difference between the single universal level at $L_z^A = 64$ and the lowest generic level at the same L_z^A (see Fig. 7). In addition, we track the difference between the lowest two levels at $L_z^A = 56$, which is the symmetry point between the MR Pfaffian and aPf spectra (see the top panel of Fig. 6) and also appears to be the lowest L_z^A "universal" level after the first phase transition ($\kappa \approx 0.66$).

In Fig. 8, we show the topological gap in the Pfaffian-like phase for different widths along with the $L_z^A = 56$ gap at $w/\ell_0 = 0$. We observe that the topological gap remains relatively robust to the variations of finite thickness and Landau-level-mixing strength for small κ. For each width, there exists a critical value of κ that can be approximately inferred from the MR Pfaffian overlap, where the topological gap vanishes. We see that the $L_z^A = 56$ gap displays a sharp jump simultaneous with the vanishing of the MR Pfaffian topological gap at $w = 0$. The vanishing of the topological gap may indicate a topological phase transition where the new state is also topological but has opposite chirality. We further discuss this state in Sec. VIII. With increasing Landau-level-mixing strength, the $L_z^A = 56$ gap is suppressed until a different phase appears around $\kappa = 0.73$.

We also study the dependence of the MR Pfaffian topological gap on the system size for N_Φ up to 29 (not shown). System-size dependence is similar to the one presented in Ref. [76] with the smaller systems developing
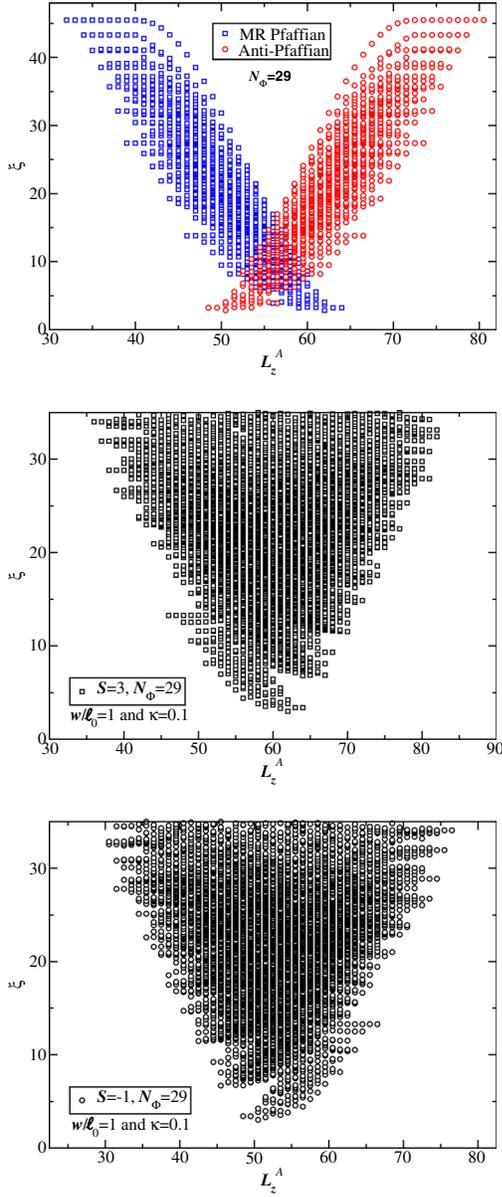
FIG. 7.   Entanglement spectrum for $N_\Phi = 29$ at $\kappa = 0.2$, 0.53, 0.66, and 0.73. The entanglement spectra at $\kappa = 0.2$ and 0.53 are shown in blue to emphasize their consistency with a ground state in the universality class of the MR Pfaffian. At $\kappa = 0.66$, we show the entanglement spectra between the two entanglement entropy peaks in the lower panel of Fig. 13. It is colored red to indicate that its low-lying level structure has some similarity to states in the aPf universality class, although the entanglement gap is too small to allow for any definitive statements. At $\kappa = 0.73$, the entanglement spectrum completely changes to that of the unknown phase to the right of the second entanglement entropy peak in Fig. 13. We also indicate the definition of the "topological gap" for $\kappa = 0.2$, 0.53, and 0.66 as described in the text.

FIG. 6.   The entanglement spectra for the MR Pfaffian (blue squares) and aPf (red circles) on the sphere at $S = 3$ and $S = -1$, respectively, are shown in the top panel. The MR state has a negative slope (discussed more in the text), while the aPf has a positive slope. The middle and lower panels show the entanglement spectrum for the exact ground state at $S = 3$ and $S = -1$, respectively, for $\kappa = 0.1$ and $w/\ell_0 = 1$. At $S = 3$, the low-lying states show the same slope and level structure as the MR state, and at $S = -1$, they show the same slope and level structure as the aPf state. Both systems are at $N_\Phi = 29$ and are partitioned to have 15 orbitals in each hemisphere. (The partitioning corresponds to the partition of $P[0|0]$ in the notation of Li and Haldane [76].)

large finite-size effects for higher κ. Reasonable extrapolation to the thermodynamic limit is therefore only possible for $\kappa \leq 0.45$, where we see that the extrapolated topological gap remains finite and relatively robust to the variation of the Landau-level-mixing strength.
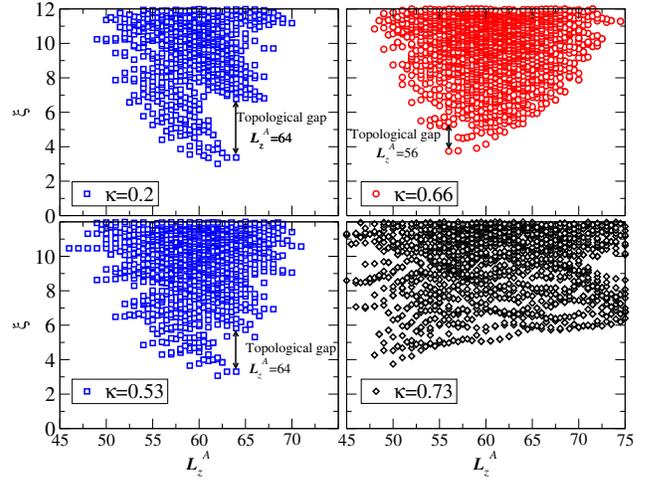

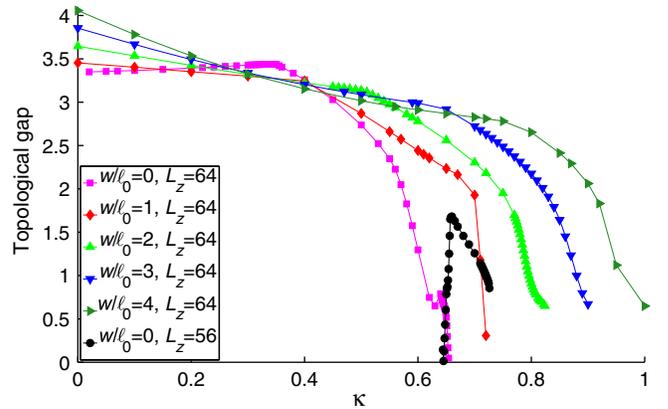FIG. 8.   The topological gap, the difference between the universal and lowest generic level at $L_z^A = 64$, is calculated in spherical geometry at $S = 3$ for the system with $N_\Phi = 29$. Note that qualitatively the behavior and collapse of the topological gap are similar to the collapse of the overlaps shown in Fig. 5. We also show the topological gap at $L_z^A = 56$ (filled black circles) in the region of parameter space where the entanglement spectrum qualitatively changes and has the same chirality as the aPf state (see the $\kappa = 0.66$ panel in Fig. 7).

VI. ENERGY GAPS

We now turn to the energy gap and show that the gap collapses as κ is increased, mirroring the collapse of the wave-function overlap, thereby justifying the claim that the latter signals the onset of a phase transition. There are several different energy gaps in a fractional quantum Hall system, with different experimental manifestations. The simplest gap, which we will simply call the "energy gap," is the difference in energy between the two lowest eigenvalues of the Hamiltonian, for a fixed particle number. This gap must become small (i.e., vanishing in the thermodynamic limit) at a phase transition. Hence, it is the appropriate quantity to compute when looking for a phase transition. However, the energy gap may not be relevant to transport experiments, which are insensitive to the gap to neutral excitations. The transport gap is typically deduced in one of two ways, which we discuss in Appendix B. For reasons that are explained there, we primarily use the so-called "exciton gap" to estimate the transport gap. As shown in Fig. 15 in Appendix B, the various different ways of computing the transport gap are broadly consistent, although there are quantitative differences. In Appendix B, we also establish the connection to previous important work [77] that estimated the transport gap in the spherical geometry with $S = 3$ including finite thickness but neglecting Landau-level mixing.

The dependence of the energy gap on κ and w/ℓ_0 is shown in Fig. 4. The gaps at $S = 3$ and $S = -1$ both decrease monotonically with κ and collapse to 0 at approximately the same value of κ, coinciding with the vanishing of the overlaps. ($\kappa \sim 0.7$–1.0, depending on the width, with larger widths corresponding to larger critical κ's.) The energy gap behavior supports the conclusion that the decrease of the overlap signals the approach to a phase transition, rather than just a failure of the trial wave functions.

Moreover, the energy gap is larger at $S = 3$ than at $S = -1$ for most Landau-level-mixing strengths. If the true ground state of the system were at $S = 3$, then we would expect that, in the thermodynamic limit, there would be no gap at $S = -1$ since the lowest energy state at shift -1 would be a state with eight charge-$e/4$ quasiholes, leading to gapless excitations. The reduction of the gap at $S = -1$ relative to the gap at $S = 3$ is consistent with the above scenario, but the fact that it is not 0 indicates that we may not be seeing the asymptotic behavior of the system. For instance, while the aPf ground state must have higher energy than the MR ground state (assuming that the latter is the ground state) by an extensive energy difference, it may still have lower energy than the MR state with eight quasiholes at these system sizes. There are numerical indications that the size of the quasiholes is on the order of many magnetic lengths. Therefore, they may strongly overlap at these system sizes, thereby leading to a finite gap for finite-size systems [78]. Hence, the extrapolation to the thermodynamic limit might be a much more delicate

procedure then previously appreciated and, in fact, could point to a potential reason for the long-noticed discrepancy between calculated energy gaps and experimentally measured gaps [2–10,12,14–23].

To provide qualitative guidance to the experiment and to connect to the previous gap estimates in the literature, we show in Fig. 9 our estimates of the exciton gap extrapolated to the infinite system size. Our results show that Landau-level mixing and finite thickness have a nontrivial interplay in the second Landau level. Landau-level mixing reduces the energy gaps more significantly than finite thickness alone. But, we find that both effects, taken together, produce a further reduction. Our results are in direct contrast to what has been found in the lowest Landau levels [79,80] where both effects were not found to be additive.

Our results show that Landau-level mixing lowers energy gaps, thereby bringing theoretical estimates closer to experimental measurements [2–10,12,14–23] of the transport gap. Furthermore, the strong suppression of the gap as a function of the Landau-level-mixing strength that we observe is in good qualitative agreement with experimental findings presented in Fig. 4 of Ref. [81]. There, four different experiments are analyzed following the idea originally suggested in Ref. [82], and a similar trend for the dependence of the intrinsic (disorder-corrected) gap on the κ parameter is found. Based on the experimental evidence, the authors come to the conclusion that "the $\nu = 5/2$ fractional quantum Hall state should not develop for $\kappa > \kappa_{\text{th}}$." The suggested absence of a fractional quantum Hall state is in agreement with our
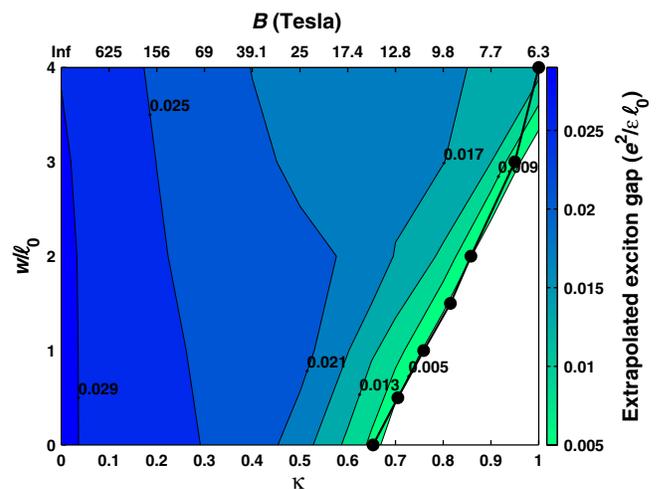

FIG. 9. Color map of the extrapolated exciton gap at $S = 3$ versus both well width and κ. The contours show specific values of the extrapolated exciton gap. Note that the extrapolation becomes less reliable when approaching the phase transition. The black circles show the transition border determined by the first peak in the entanglement entropy for $N_\phi = 29$ on the sphere (discussed in Sec. VIII). We do not extrapolate the exciton gap after the phase transition (white area). The top x axis is the magnetic field for GaAs samples.

findings that gaps and trial wave-function overlaps vanish beyond some critical Landau-level-mixing strength that we cannot predict precisely due to the fact that our effective Hamiltonian is, strictly speaking, only valid for small κ.

In Appendix A, we demonstrate that the width of an infinitely deep quantum well w provides a reasonable parametrization for the finite-width effect. In order to compare with the experiment, one should find the variance of the electron wave function in the direction perpendicular to the two-dimensional electron gas in the specific heterostructure (for instance, by means of a coupled Schrödinger-Poisson solver in 1D). Infinite quantum-well width w leading to the same variance should be taken. Note that the width w is given in Fig. 9 in units of magnetic length and therefore depends on the magnetic field since $\ell_0 \approx 25$ nm$/\sqrt{B[T]}$, where $B[T]$ is the magnetic field in Tesla.

VII. PARTICLE-HOLE SYMMETRY-BREAKING ORDER PARAMETER

States in the MR and aPf universality classes cannot be invariant under particle-hole symmetry. Indeed, under a particle-hole transformation, a state in the MR universality class is transformed into a state in the aPf universality class [53,54]. Thus, if we consider an operator ϕ that is odd under a particle-hole transformation, then $\langle\phi\rangle \equiv \langle\Psi_{\text{trial}}|\phi|\Psi_{\text{trial}}\rangle$ must have one sign in any state in the MR universality class and the opposite sign in any state in the aPf universality class, assuming that $\langle\phi\rangle$ vanishes only in states that are symmetric under particle-hole symmetry (i.e., excluding, through a judicious choice of ϕ, the possibility that $\langle\phi\rangle$ vanishes "accidentally"). We choose the order parameter to be built from the operator that is conjugate to the variable κ that controls the particle-hole symmetry breaking. This operator is $H_{\text{3body}} = \sum_m V_m^{(3)}(w/\ell_0, \kappa) \sum_{i<j<k} \hat{P}_{ijk}(m)$. Note that κ can be pulled out of this expression completely since H_{3body} is linear in κ; hence, we can write $H_{\text{3body}} = \kappa H'_{\text{3body}} = \kappa \sum_m V_m^{(3)}(w/\ell_0, 1) \sum_{i<j<k} \hat{P}_{ijk}(m)$. The order parameter is then taken to be

$$\phi \equiv \frac{1}{2}\left(H'_{\text{3body}} - \overline{H'_{\text{3body}}}\right), \qquad (5)$$

where the overline denotes particle-hole conjugation.

To demonstrate this definition, let us consider a model that interpolates adiabatically between the pure Coulomb Hamiltonian and the Hamiltonians whose ground states are in the MR and aPf universality classes. That is, $(1-\alpha)H(0,0,1) + \alpha H_3$ or $(1-\alpha)H(0,0,1) + \alpha\overline{H_3}$, where $H_3 \equiv \sum_{i<j<k} \hat{P}_{ijk}(m = 3)$ is the Hamiltonian that generates the MR wave function as an exact zero-energy ground state and $\overline{H_3}$ is its particle-hole conjugate and generates the aPf wave function. For this model, we take the order parameter to be $(H_3 - \overline{H_3})/2$ since H_3 is the operator that breaks the particle-hole symmetry by increasing the

variable α. The expectation value of this operator has sign $\langle\Psi_{\text{MR}}|\phi|\Psi_{\text{MR}}\rangle < 0$ and $\langle\Psi_{\text{aPf}}|\phi|\Psi_{\text{aPf}}\rangle > 0$, and changes sign in the expected manner, as shown in Appendix C. Therefore, we expect the above definition of ϕ [Eq. (5) for the Landau-level-mixing Hamiltonian] will show similar behavior and $\langle\phi\rangle$ will be negative (positive) for an eigenstate in the MR (aPf) universality class.

We first examine this operator in the system in which it is most straightforward. Recall that on the torus the MR and aPf states occur at the same flux. Here, $\langle\phi\rangle$ is particularly useful in determining the universality class of the ground state of Eq. (2). The expectation of ϕ in the ground state is the most important quantity, but we will focus on the lowest and first excited eigenstates on the torus with a hexagonal unit cell containing an odd number of electrons as a function of κ for $w/\ell_0 = 0$. In Fig. 10, we show the expectation value of ϕ in the ground and first excited states for $N_\Phi = 18$, 22, and 30. These results clearly show that the ground state breaks particle-hole symmetry in the same way as the MR state and $\langle\phi\rangle < 0$. Moreover, the expectation value of ϕ in the first excited states is positive and, therefore, breaks particle-hole symmetry in the same way as the aPf state.

In Fig. 10, it is observed that $\langle\phi\rangle \neq 0$ for $\kappa = 0$. The hexagonal unit cell has an exact degeneracy for $\kappa = 0$ for an odd number of electrons in the unit cell, as discussed above in Sec. IV. At $\kappa = 0$, there is a basis in which one of the degenerate states has positive $\langle\phi\rangle$ and the other state has a negative value. This basis evolves smoothly into the $\kappa > 0$ eigenstates. However, we could just as easily take the symmetric and antisymmetric combinations of these two degenerate states, and these combinations would respect the particle-hole symmetry and have vanishing $\langle\phi\rangle$. For an
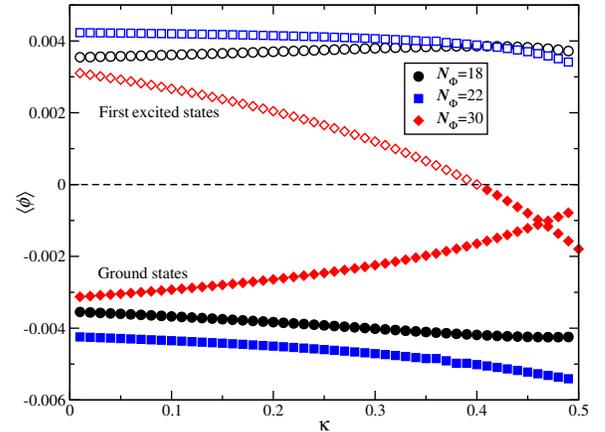

FIG. 10. The expectation value of a particle-hole-antisymmetric order parameter ϕ for the ground state and first excited state of Eq. (2) on the torus using the hexagonal unit cell for $N_\Phi = 18$, 22, and 30 as a function of κ for $w/\ell_0 = 0$. The ground state is consistent with the MR state and has $\langle\phi\rangle < 0$ (filled symbols), while the first excited state is consistent with the aPf state with $\langle\phi\rangle > 0$ (open symbols).

even number of electrons per unit cell, where the degeneracy is not exact at $\kappa = 0$, the energy splitting between the symmetric and antisymmetric combinations is nonzero due to tunneling in a finite-sized system, and the ground state at $\kappa = 0$ is the symmetric combination, with $\langle \phi \rangle = 0$.

Next, we consider $\langle \phi \rangle$ in the spherical geometry. Here, we fix $N_\Phi = 2N_e - 1$ to be the particle-hole-symmetric point since the shift S explicitly breaks particle-hole symmetry and we want to observe this symmetry breaking due to Landau-level-mixing effects. Figure 11 shows the order parameter for the ground state at $N_\Phi = 13, 15, 17, 19$, and 21 for various w/ℓ_0 as a function of κ. Here, the order parameter vanishes for $\kappa = 0$ and increasing κ drives the system into the MR universality class and $\langle \phi \rangle$ becomes more negative for increasing κ.

Finally, we investigate the lowest few energy eigenstates of Eq. (2) in the torus geometry using the hexagonal unit cell for N_e odd in Fig. 12. States with negative (positive) order parameter are indicated by a filled (open) symbol. The first excited state has $\langle \phi \rangle > 0$, but the rest have $\langle \phi \rangle < 0$. Thus, although the second, third, fourth, and fifth excited states look like an exciton on the MR ground state, in that they have a negative expectation value of the order parameter and therefore belong in the MR universality class, the first excited state does not. It, instead, looks like
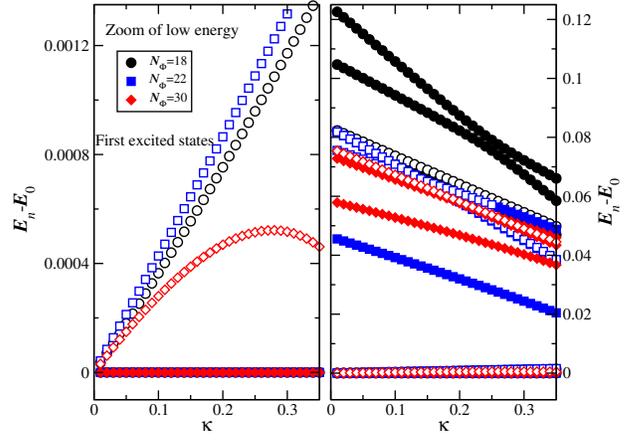
FIG. 12. The total energies relative to the ground-state energy on the torus using the hexagonal unit cell for $N_\Phi = 18, 22$, and 30 as a function of κ for $w/\ell_0 = 0$. Similar to Fig. 10, a state with $\langle \phi \rangle < 0$ has a filled symbol while a state with $\langle \phi \rangle > 0$ has an open symbol. The right panel shows the six lowest eigenstates. We have zoomed in on the lowest two eigenstates in the left panel. While many of the higher-energy excitations look like they belong to the MR universality class according to $\langle \phi \rangle$, the first excited state looks like an aPf ground state rather than an excitation above a MR ground state, unlike the other low-lying excited states. Note that the energy scale is much larger in the right panel, so the ground and first excited states are not resolvable there.

the aPf state which is consistent with conclusions from the overlaps but can only occur in small systems.

VIII. ENTANGLEMENT PROPERTIES AND PHASE DIAGRAM

From the preceding calculations, we have seen the following concomitant behaviors: a sharp drop in the energy gap, a corresponding drop in the overlap between the ground state and the MR wave function, and a negative expectation value of a particle-hole symmetry-breaking order parameter. The energy gap vanishes at the phase transition to a competing phase.

This phase-transition point can also be identified by computing the bipartite entanglement entropy, which is the von Neumann entropy of the reduced density matrix [71–75], discussed in Sec. V. Figure 13 shows that the resulting entanglement entropy displays two nearby peaks as a function of κ (only a single peak for $w/\ell_0 > 1.5$). The position of the two peaks coincides with the vanishing of the overlap, which, in turn, coincides with the vanishing of the energy gap, as per Fig. 4. These peaks in the entanglement entropy indicate phase transitions [83].

In the bottom panel of Fig. 13, we see that there are two distinct peaks in the entanglement entropy at $w/\ell_0 = 0$, while in the top panel, we see that the two peaks are barely distinguishable at $w/\ell_0 = 1$. Intriguingly, the ground state has higher overlap with the aPf wave function
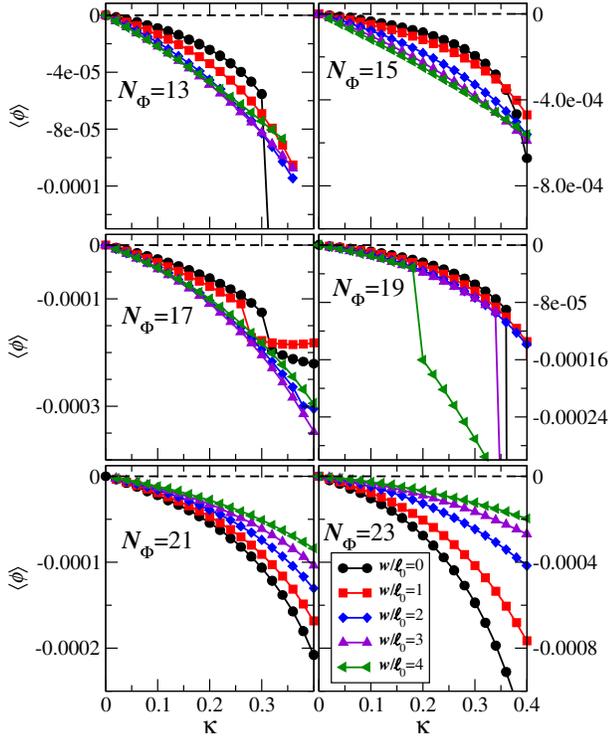

FIG. 11. The expectation value of the particle-hole-antisymmetric order parameter for the ground state of Eq. (2) in the spherical geometry at the particle-hole-symmetric shift $N_\Phi = 2N_e - 1$ for $N_\Phi = 13, 15, 17, 19, 21$, and 23 as a function of κ for $w/\ell_0 = 0$–4. Note that the y axis is not the same scale for each system size.
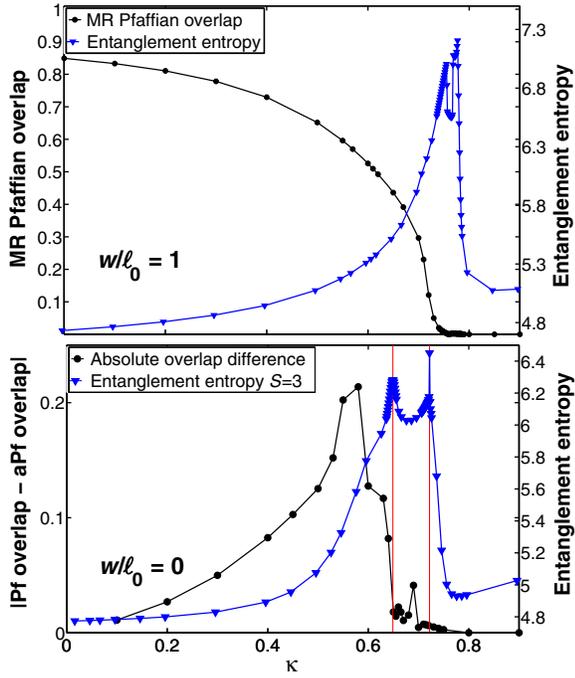
FIG. 13. Top panel: Entanglement entropy and wave-function overlap with the MR state for width $w/\ell_0 = 1$. Bottom panel: Entanglement entropy and the absolute difference of the MR Pfaffian and aPf overlaps for width $w/\ell_0 = 0$. In both cases, the spherical geometry is used with $N_\Phi = 29$ and $S = 3$. The vertical red lines in the bottom panel are just a guide to the eye to indicate the peaks in the entanglement entropy.

in the intermediate phase between the two entanglement entropy peaks although both overlaps are quite small. We speculate about the cause for the higher overlap with the aPF in Sec. IX.

It is instructive to discuss the nature of all the phases mentioned in relation with the corresponding entanglement spectra for $w/\ell_0 = 0$ shown in Fig. 7. Comparing the spectra at $\kappa = 0.2$ and $\kappa = 0.53$ in Fig. 7 (upper and lower left panels), we observe that, with increasing Landau-level-mixing strength, the universal part of the entanglement spectrum gets absorbed by the "generic" spectrum above it, which leads to a decrease of the "topological gap" [76] as shown in Fig. 8.

Between the two peaks of entanglement entropy, at approximately $\kappa = 0.66$, the low-lying levels of the spectrum have positive slope (upper right panel of Fig. 7). The positive slope indicates that in this phase, there exists an edge mode propagating in the direction opposite to the MR Pfaffian edge. However, both the energy gap and entanglement gap are quite small, so to say anything definitive about this state would require much larger system sizes (compared to what is currently available using exact diagonalization). In the phase diagram shown in Fig. 14, this state is located between the two black lines indicating the entropy peaks.

The entanglement spectrum for stronger Landau-level mixing has a completely different nature, as shown in the
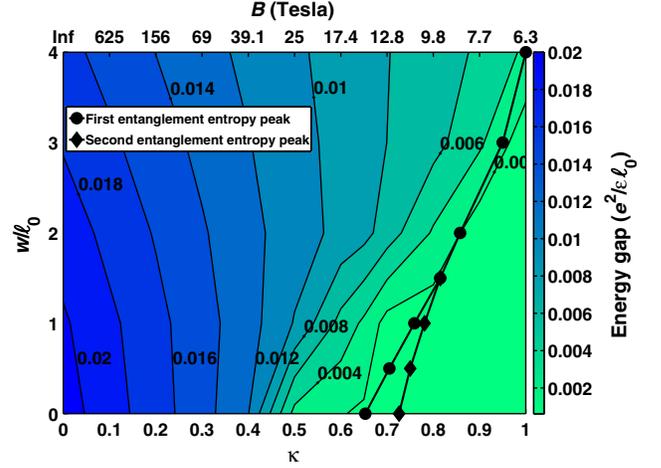

FIG. 14. Quantum phase diagram obtained from a color map of the energy gap (difference between the two lowest eigenstates for the system with $N_\phi = 33$) plotted versus well width and κ. Contours plot specific values of the extrapolated gap. Lines with black circles and black diamonds show the positions of the entanglement entropy peaks for $N_\phi = 29$ and represent the approximate phase boundaries. All the states to the left from the line connecting the black circles belong to the MR Pfaffian universality class. The top x axis is the magnetic field for GaAs samples. All results are obtained on the sphere.

bottom right panel of Fig. 7. We defer the discussion of this regime to later work.

Finally, we discuss an approximate quantum phase diagram (QPD) for the fractional quantum Hall effect at $\nu = 5/2$ in Fig. 14. The QPD is determined with two distinct measures: energy gap and entanglement entropy. The energy gap depicted is for the largest system with $N_\Phi = 33$ while the entanglement entropy is for $N_\Phi = 29$. Figure 14 shows a contour plot of the energy gap for $S = 3$, as functions of κ and w/ℓ_0. We also indicate the position of the first peak in the entanglement entropy (black circles), clearly showing that it occurs where the energy gap becomes very small for $N_e = 18$ (presumably indicating that it vanishes in the thermodynamic limit). The results presented in Fig. 14 are in agreement with overlaps with the MR state as well. This QPD can serve as a guide for experimental searches for the robust fractional quantum Hall effect at $\nu = 5/2$ and is the first approximate QPD calculated at $\nu = 5/2$ including both Landau-level mixing and finite width.

IX. CONCLUSIONS

Our results demonstrate that the $\nu = 5/2$ state for small nonzero κ and $0 \leq w/\ell_0 \leq 4$ is in the universality class of the Moore-Read Pfaffian state. In the small-κ limit, our approximations are controlled: We use the correct Hamiltonian to $O(\kappa)$, and all corrections to our Hamiltonian are of higher order in κ and, therefore, can be neglected for sufficiently small κ. Our results are in qualitative agreement

with the results of Ref. [48]. We reached our conclusion by computing several properties of the ground state. They all validate the use of overlaps in this case. Our results are in disagreement with the results of Ref. [47], which found a ground state in the aPf universality class.

Finite-size effects might be a potential source of error in our study. One source of finite size errors may arise from the fact that we are using, in a finite system, pseudopotentials that were originally derived for the infinite system. The use of infinite system size pseudopotentials should make no difference for sufficiently large systems and, therefore, in the thermodynamic limit. However, it can affect our ability to make an extrapolation from small systems to the thermodynamic limit. Hence, we have checked the perturbative contribution to the energy difference using size-dependent spherical pseudopotentials in Appendix D; our results are qualitatively unchanged.

Finally, the phase that emerges at κ just larger than the gap closing is an interesting open problem. The energy gap and the entanglement gap are too small for us to say anything reliable at present. However, the overlap with the aPf is larger than the overlap with the MR state and the entanglement spectrum is consistent with a counterpropagating edge mode, so it is possible that the aPf state occurs in this narrow window, albeit with much smaller energy gap (possibly more in line with experimental gap values). In this context, we note that the experiment of Bid *et al.* [84] found evidence for a counterpropagating neutral mode in a $\nu = 5/2$ state at $B \approx 5T$ ($\kappa \approx 1.12$), consistent with the anti-Pfaffian state, which supports the scenario that a different $5/2$ state occurs at larger κ and that this state is the anti-Pfaffian. Another possibility is a strong pairing phase [63].

Note that small κ corresponds to relatively high magnetic fields; e.g., $\kappa = 0.5$ is a magnetic field of 25 T for GaAs samples. The range of magnetic fields and quantum-well widths over which there is a $\nu = 5/2$ state in both experiments and our numerics is the range $6 \text{ T} \leq B \leq 12 \text{ T}$ and $w/\ell_0 \sim 2$–4. For $B \lesssim 6$ T, we do not find a quantum Hall state at $5/2$ even though experiments see a $5/2$ plateau all the way down to $B \sim 1$–2 T [12,21]. There are two distinct possible explanations for this discrepancy between our results and experiments.

One is that our effective Hamiltonian is simply not quantitatively correct for $\kappa \gtrsim 1$, and including higher-order corrections in κ would shift the phase transition to lower magnetic fields. While we do not know the precise Landau-level-mixing strength κ beyond which our effective Hamiltonian is no longer valid, the large-κ discrepancy between our results and experiments indicates that higher-order corrections become important in the vicinity of $\kappa = 0.6$. Nevertheless, we choose to also present the results of our model at higher κ since they may still correctly capture the trends in the κ dependence and since they will be useful guidance and motivation for the future studies attempting to incorporate higher-order corrections and

thus understand the nature of the incompressible state at low fields. Additionally, we note that for widths beyond $w/\ell_0 \gtrsim 5$, real experimental systems are often better described as two-component systems.

The other possibility is that some of the experimental observations at low fields are spin-unpolarized states—a possibility that we have ignored in this work since we have assumed that the system is fully spin polarized. Although there exist experimental studies [85] that demonstrate the spin-polarized nature of the $5/2$ state for a certain magnetic field and finite width, these studies do not exclude the possibility that there exists a spin-unpolarized incompressible region of the phase diagram that has not been probed by NMR. It is an open question as to the effect of Landau-level mixing and finite width have on the spin polarization and whether the ground state, if unpolarized, is or is not in the universality class of the MR Pfaffian or aPf phase. These questions will have to await future studies.

Our results demonstrating the strong suppression of the gap by Landau-level mixing are in good qualitative agreement with the experimental observations [81] and should in turn motivate the experimental community searching for a non-Abelian phase to explore higher magnetic fields where a more stable $5/2$ state in the MR Pfaffian universality class is predicted by our model.

ACKNOWLEDGMENTS

APPENDIX A: MODELS FOR NONZERO WIDTH

We include nonzero width of the two-dimensional electron system using two approaches. In the first approach, we, for $\kappa \neq 0$, assume that the electrons are confined to an infinitely deep square quantum well in the z direction so that the z dependence of the wave function for the nth subband is $\phi_n(z) = \sqrt{2/w}\sin[(n+1)\pi z/w]$ with $z \in [0, w]$ and subband energy $\epsilon_n = (n+1)^2\pi^2\hbar^2/(2m_z w^2)$. Here, m_z is the effective electron mass in the quantum well (see Ref. [59] for details).

In the second approach, we choose an alternative Gaussian model to demonstrate that the above choice of the finite thickness model does not change our results qualitatively or quantitatively. We fix $\kappa = 0$ and take the z dependence to have a Gaussian form $\phi(z) = (\sigma^2 2\pi)^{-1/4}e^{-z^2/4\sigma^2}$. (This wave function is the solution of a parabolic potential, but since we use it only for $\kappa = 0$, we do not consider any subband-mixing effects.)

Figure 15 shows that the energy gaps (extrapolated to the thermodynamic limit) are very similar for both models of nonzero width. To compare each model at a similar width, we consider each energy gap as a function of the variance of the wave functions $\text{var} = \sqrt{\langle z^2 \rangle - \langle z \rangle^2}$; that is, $\text{var} = \sigma/\ell_0$ for the Gaussian wave function and $\text{var} = 0.180756(w/\ell_0)$ for the infinite square-well wave function.
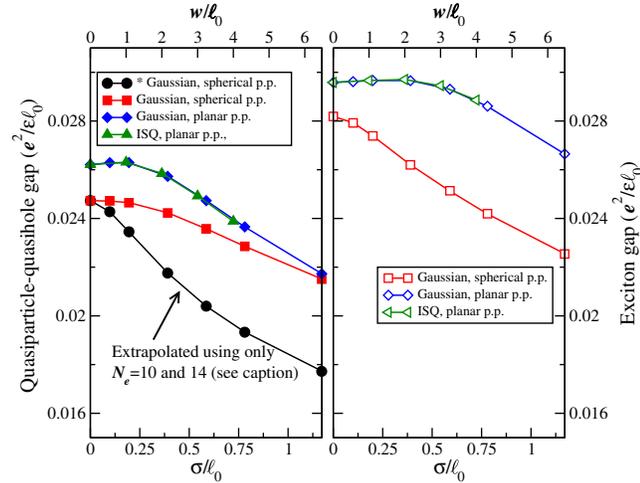

FIG. 15.   Extrapolated quasiparticle-quasihole (left panel, filled symbols) and exciton (right panel, open symbols) energy gaps as a function of well width. Each gap is calculated with spherical and planar pseudopotentials (p.p.) for two different models of the finite thickness, Gaussian, and infinite square well (ISQ); see Appendix A. The solid black circles (marked in the legend with an asterisk) are the same as the solid red squares but are obtained from an extrapolation of only $N_e = 10$ and 14 electrons. The solid black circles reproduce the width dependence obtained in Ref. [77] [Fig. 14(b)] to show that using more particles in the extrapolation (the other data points use $N_e = 10$, 14, and 18 electrons) leads to larger gaps.

APPENDIX B: EXCITON AND QUASIPARTICLE-QUASIHOLE GAPS

To estimate the gap on the sphere in the thermodynamic limit, we generally follow Ref. [77]. We take energy differences and perform a linear (in $1/N_e$) extrapolation to infinite system sizes after we convert the energy difference by using the magnetic length in the infinite system [77]. We calculate energy difference (and therefore the gap) in two distinct ways.

(i) The exciton gap is the energy difference between the ground and the lowest excited state with total angular momentum $L = N_e/2$ or $L = N_e/2 - 1$ for $N_e/2$ even or odd, respectively. This excited state contains a quasiparticle and quasihole, maximally separated on the sphere [77]. The quasiparticle and quasihole are assumed to have charges $\mp e/4$ and to be separated by the diameter of the sphere $2\sqrt{N_e}\ell_0$, so we subtract the energy of the quasiparticle-quasihole ideal Coulomb attraction $-\frac{1}{32}(1/\sqrt{N_e})$. [This energy contribution is $A_{q=1/4}(\nu = 1/2)$ in Ref. [77].] This exciton gap is calculated for $N_e = 8, 10, 14, 16, 18$. ($N_e = 12$ is aliased with a composite fermion state at $\nu = 3/5$ and is ambiguous [70].) Note that the background energy does not enter into this definition of the gap since its contribution explicitly cancels.

(ii) Alternatively, one can compare the ground-state energy at N_Φ to the ground-state energies with one additional or fewer flux quantum. The states with an additional or missing flux quantum are states with two quasiholes or two quasiparticles, respectively. While more subtle than in the case of the exciton gap, the background energies cancel again. The resulting gap, sometimes called the quasiparticle-quasihole (qp-qh) gap [77], is calculated for $N_e = 10$, 14, and 18. Other system sizes are aliased (see Table 3 in Ref. [77]).

Although we present both gap calculations, we consider the exciton gap a more reliable gap estimate in the thermodynamic limit due to the less severe aliasing problem. Only estimates using the exciton gap are used in the main text.

In Fig. 15, we illustrate the differences between the various ways of calculating the thermodynamic limit of the energy gap. The gap is roughly the same for an infinite square-well potential as it is for a Gaussian z dependence (once they are taken such that the wave-function variance is the same) and for spherical and planar pseudopotentials. However, there are some quantitative differences: (i) If one extrapolates based on larger system sizes, the width dependence of the qp-qh gap is less pronounced and can only account for a 13% decrease of the gap compared to 28%; (ii) although in agreement qualitatively, using planar pseudopotentials instead of spherical ones tends to give higher gap estimates; and (iii) the exciton gap is larger than the qp-qh gap.

APPENDIX C: PARTICLE-HOLE SYMMETRY-BREAKING ORDER PARAMETER FOR AN ILLUSTRATIVE MODEL HAMILTONIAN

In Sec. VII, we introduced an order parameter [Eq. (5)] for particle-hole symmetry breaking. We now show that this order parameter has negative expectation value in the MR trial wave function and positive expectation value in the aPf trial wave function. Figure 16 shows $\langle \phi \rangle$ for the ground state of $(1-\alpha)H(0,0,1) + \alpha H_3$ and the ground state of $(1-\alpha)H(0,0,1) + \alpha \overline{H_3}$. Here, $H_3 \equiv \sum_{i<j<k} \hat{P}_{ijk}(m = 3)$ and $\overline{H_3}$ is the particle-hole conjugate of H_3. As may be seen from the $\alpha \to 1$ behavior in Fig. 16, when the ground state is in the MR universality class, $\langle \phi \rangle < 0$ and when it is the aPf wave function, $\langle \phi \rangle > 0$. Moreover, the order parameter interpolates smoothly between 0 and these values, as α is increased from 0.

These calculations are performed on the sphere and on the torus for comparison. For the spherical geometry, $\langle \phi \rangle$ is calculated at $N_\Phi = 2N_e - 1$, which is the particle-hole-symmetric value of the shift on the sphere. Thus, at $\alpha = 0$, there is no particle-hole symmetry breaking due to finite-size effects. At $N_\Phi = 2N_e - 1$, the ground state of H_3 is not the MR wave function but the MR wave function with four MR quasiholes, and the ground state of $\overline{H_3}$ is the aPf wave function with four aPf quasiparticles. On the torus, we use the rectangular unit cell and show the results for the corner of the Brillouin zone for $N_e = 8$ electrons, i.e., $\mathbf{K} = (N_0/2, N_0/2)$. The other K points corresponding to the MR state display similar behavior. Note in the

rectangular cell, we find $\langle \phi \rangle = 0$ for $\alpha = 0$, while in the hexagonal unit cell, for an even number of electrons, this is not the case.

APPENDIX D: FINITE-SIZE EFFECTS, PLANAR AND SPHERICAL PSEUDOPOTENTIALS, AND $m > 8$ PSEUDOPOTENTIALS

In our model Hamiltonian, we use planar pseudopotentials. Although spherical pseudopotentials approach planar ones in sufficiently large systems, our use of planar pseudopotentials can be a source of systematic error in small spherical systems. In this section, we analyze the differences between spherical pseudopotentials and the planar ones used in the results reported in Sec. III. We also perform an extrapolation in system size to ensure our conclusions hold in the thermodynamic limit. We restrict our discussion here to small κ, which is the limit in which our Hamiltonian is exact on the plane.

To consider the effect of planar versus spherical pseudopotentials in Eq. (2), we compute the spherical pseudopotentials using a program kindly provided by Steve
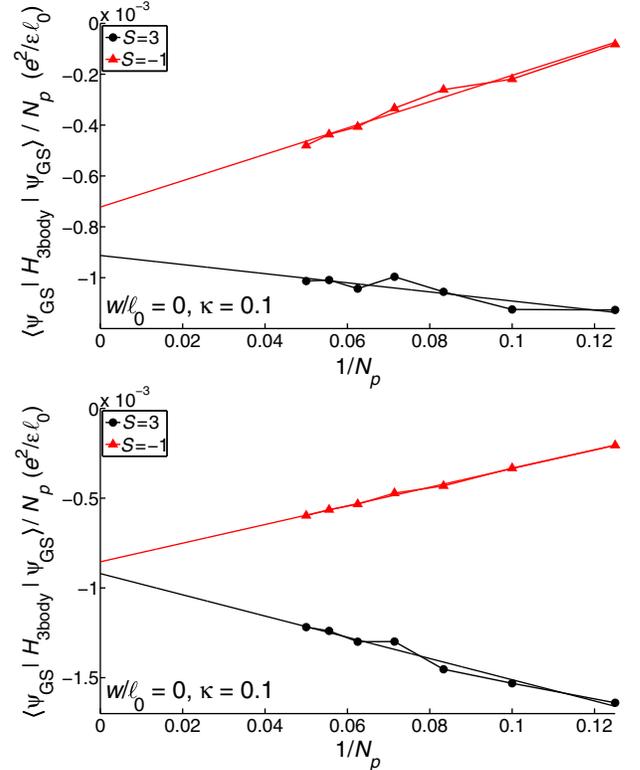
FIG. 17. Three-body energy contributions are calculated with system-size-dependent (bottom panel) and extrapolated (top panel) spherical pseudopotentials. The energy differences between the extrapolated values are $0.000066e^2/\epsilon\ell_0 = 0.045\kappa|V_3^{(3)}|$ (bottom panel) and $0.00019e^2/\epsilon\ell_0 = 0.13\kappa|V_3^{(3)}|$ (top panel). Although relatively small, these values are per particle and should thus provide extensive energy separation between the two states in the thermodynamic limit.
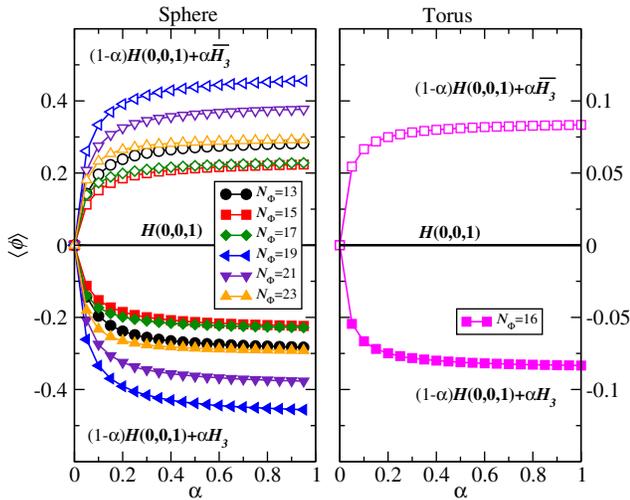

FIG. 16. Left: The particle-hole-antisymmetric order parameter computed for Hamiltonians in the spherical geometry that interpolate between the $N = 1$ Landau-level Coulomb Hamiltonian $H(0,0,1)$ at $\alpha = 0$ and the Hamiltonians H_3 (solid symbols) and $\overline{H_3}$ (open symbols), respectively, for systems with $N_\Phi = 13$–21 corresponding to $N_e = 7$–11. Right: The same but computed on the torus using a rectangular unit cell for $N_e = 8$.

FIG. 18.   Top panel: Expectation value of the three-body terms in the MR and aPf trial wave functions as a function of angular momentum m, i.e., $\langle \Psi_{\text{trial}} | H_{3\text{body}}(m) |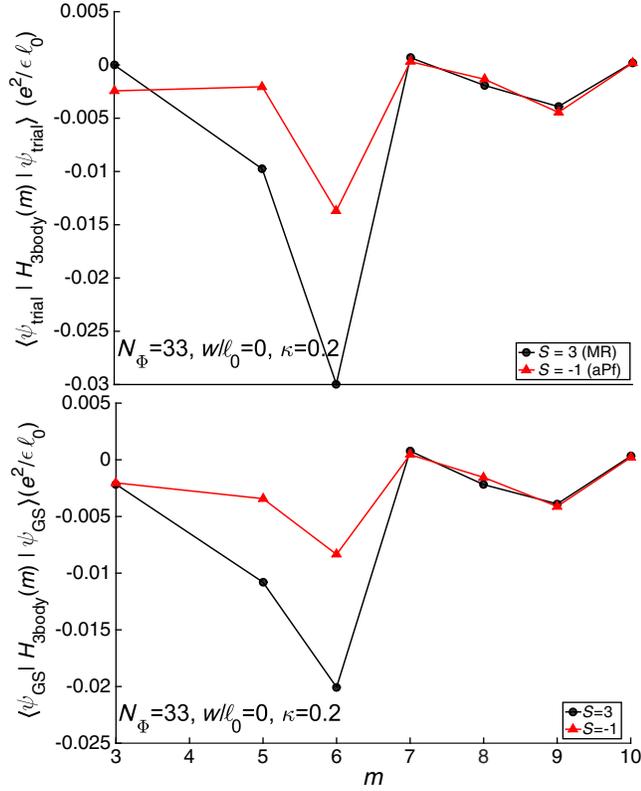 \Psi_{\text{trial}} \rangle$ where $H_{3\text{body}}(m) = V_m^{(3)}(w/\ell_0, \kappa) \sum_{i<j<k} \hat{P}_{ijk}(m)$, and $\Psi_{\text{trial}} = \Psi_{\text{MR}}$ or Ψ_{aPf}. Bottom panel: Expectation value of the three-body terms for the $S = 3$ and $S = -1$ ideal Coulomb ground states as a function of angular momentum m.

FIG. 19.   Top panel: Energy gap (difference between the two lowest eigenvalues) calculated at the "Pfaffian" shift $S = 3$ in a system with 16 electrons. Bottom panel: MR Pfaffian overlap. Black data points correspond to the Hamiltonian used in the main text where only the three-body pseudopotentials $V_m^{(3)}$ with $m \leq 8$ are used. Red data points correspond to the case when also $V_9^{(3)}$ and $V_{10}^{(3)}$ are included.

Simon, which was also used in Ref. [61]. We obtain the spherical three-body pseudopotentials for each of our relevant system sizes along with the three-body pseudopotentials carefully extrapolated to infinite size. For our biggest systems, the pseudopotentials could not be calculated directly and we use the values obtained from extrapolation in $1/N_\Phi$. The pseudopotential dependence on $1/N_\Phi$ we find is somewhat softer than presented in Ref. [61] but has a clear linear dependence; hence, using the extrapolated values is justified. The code used [61] only gives us the differences of the pseudopotentials (e.g., $V_5 - V_3$). A constant shift of the three-body pseudopotentials does not influence the many-body state. We choose this shift so that the finite-size spherical $V_3^{(3)}$ is equal to the extrapolated planar $V_3^{(3)}$.

In Fig. 17, we display the lowest-order perturbative (per particle) energy contributions of the three-body terms of $H(w/\ell_0 = 0, \kappa = 0.1, 1)$ given in Eq. (2) using spherical pseudopotentials, rather than the planar pseudopotentials used in Fig. 2. The top panel of Fig. 17 uses the pseudopotentials obtained by extrapolating the spherical
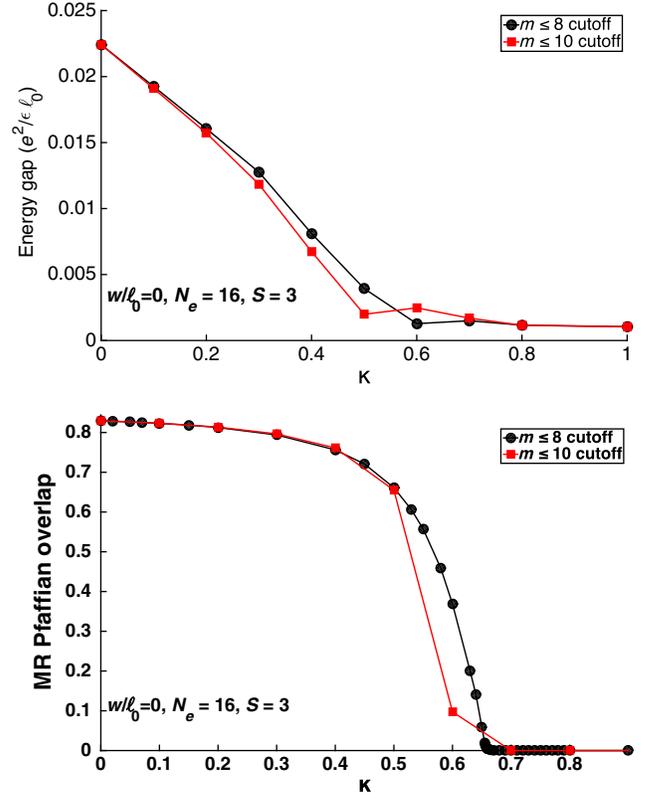
pseudopotentials to the thermodynamic limit. In principle, the result should be precisely the same as in Fig. 2, but there are small differences since the extrapolation from these system sizes does not give precisely the planar values. The lower panel, in turn, shows the same expectation values with spherical pseudopotentials used at each system size. Three-body contributions are again evaluated in the Coulomb ground state in both cases. The results are qualitatively consistent with those obtained using planar pseudopotentials: The energy is lowered more at $S = 3$ than at $S = -1$ for each individual system size as well as in the thermodynamic limit.

Finally, we estimate the importance of higher three-body pseudopotentials, not included in our effective Hamiltonian. While $V_m^{(3)}$ with $m \leq 8$ are scalar, most of the higher pseudopotentials are matrices. This fact complicates their inclusion in exact-diagonalization calculations, and we have not yet incorporated the matrix pseudopotentials. Reference [60] gives the value of $V_9^{(3)}$. To obtain a rough qualitative estimate of the expectation value for the $m = 9$ three-body pseudopotential, we use a scalar

value $-0.001025 e^2/\epsilon\ell_0$ obtained by averaging the entries of the 2×2 matrix given in Ref. [60]. The next higher three-body pseudopotential is scalar $V_{10}^{(3)} = 0.000145 e^2/\epsilon\ell_0$ and is treated exactly.

In Fig. 18, we extend Fig. 3 with results for the $m = 9$ and $m = 10$ three-body pseudopotentials, calculated as described above. We observe that both pseudopotentials do not noticeably contribute to the difference between the Pfaffian and anti-Pfaffian states and thus should not affect the central conclusion of the present work. Both expectation values are, however, nonzero, indicating that higher three-body pseudopotentials might have to be considered for quantitative comparisons to experiments.

In Fig. 19, we show the effect of the higher three-body pseudopotentials on the energy gap and on the trial wave-function overlap. We emphasize that the matrix pseudo-potential $V_9^{(3)}$ cannot be treated exactly in our code. Therefore, the data presented in Fig. 19 are an attempt to test the robustness of the ground state and to qualitatively estimate the significance of higher three-body pseudo-potentials but are not a precise representation of their effects. From these available calculations, we observe that the corrections from the higher pseudopotentials are relatively small and thus should not change the qualitative picture established using the cutoff $m \leq 8$. Precise treatment of the higher pseudopotentials may be needed if one is to exactly determine the value of κ_c, corresponding to the phase transition.

[1] R. Willett, J. P. Eisenstein, H. L. Stormer, D. C. Tsui, A. C. Gossard, and J. H. English, *Observation of an Even-Denominator Quantum Number in the Fractional Quantum Hall Effect*, Phys. Rev. Lett. **59,** 1776 (1987).

[2] R. L. Willett, H. L. Stormer, D. C. Tsui, A. C. Gossard, and J. H. English, *Quantitative Experimental Test for the Theoretical Gap Energies in the Fractional Quantum Hall Effect*, Phys. Rev. B **37,** 8476 (1988).

[3] J. P. Eisenstein, R. Willett, H. L. Stormer, D. C. Tsui, A. C. Gossard, and J. H. English, *Collapse of the Even-Denominator Fractional Quantum Hall Effect in Tilted Fields*, Phys. Rev. Lett. **61,** 997 (1988).

[4] J. P. Eisenstein, R. L. Willett, H. L. Stormer, L. N. Pfeiffer, and K. W. West, *Activation Energies for the Even-Denominator Fractional Quantum Hall Effect*, Surf. Sci. **229,** 31 (1990).

[5] W. Pan, J.-S. Xia, V. Shvarts, D. E. Adams, H. L. Stormer, D. C. Tsui, L. N. Pfeiffer, K. W. Baldwin, and K. W. West, *Exact Quantization of the Even-Denominator Fractional Quantum Hall State at $\nu = 5/2$ Landau Level Filling Factor*, Phys. Rev. Lett. **83,** 3530 (1999).

[6] W. Pan, H. L. Stormer, D. C. Tsui, L. N. Pfeiffer, K. W. Baldwin, and K. W. West, *Experimental Evidence for a Spin-Polarized Ground State in the $\nu = 5/2$ Fractional Quantum Hall Effect*, Solid State Commun. **119,** 641 (2001).

[7] J. P. Eisenstein, K. B. Cooper, L. N. Pfeiffer, and K. W. West, *Insulating and Fractional Quantum Hall States in the First Excited Landau Level*, Phys. Rev. Lett. **88,** 076801 (2002).

[8] J. S. Xia, W. Pan, C. L. Vicente, E. D. Adams, N. S. Sullivan, H. L. Stormer, D. C. Tsui, L. N. Pfeiffer, K. W. Baldwin, and K. W. West, *Electron Correlation in the Second Landau Level: A Competition between Many Nearly Degenerate Quantum Phases*, Phys. Rev. Lett. **93,** 176809 (2004).

[9] H. C. Choi, W. Kang, S. D. Sarma, L. N. Pfeiffer, and K. W. West, *Activation Gaps of Fractional Quantum Hall Effect in the Second Landau Level*, Phys. Rev. B **77,** 081301 (2008).

[10] W. Pan, J. S. Xia, H. L. Stormer, D. C. Tsui, C. Vicente, E. D. Adams, N. S. Sullivan, L. N. Pfeiffer, K. W. Baldwin, and K. W. West, *Experimental Studies of the Fractional Quantum Hall Effect in the First Excited Landau Level*, Phys. Rev. B **77,** 075307 (2008).

[11] I. Radu, J. Miller, C. Marcus, M. Kastner, L. N. Pfeiffer, and K. West, *Quasi-particle Properties from Tunneling in the $\nu = 5/2$ Fractional Quantum Hall State*, Science **320,** 899 (2008).

[12] C. R. Dean, B. A. Piot, P. Hayden, S. D. Sarma, G. Gervais, L. N. Pfeiffer, and K. W. West, *Contrasting Behavior of the 52 and 73 Fractional Quantum Hall Effect in a Tilted Field*, Phys. Rev. Lett. **101,** 186806 (2008).

[13] M. Dolev, M. Heiblum, V. Umansky, A. Stern, and D. Mahalu, *Observation of a Quarter of an Electron Charge at the $\nu = 5/2$ Quantum Hall State*, Nature (London) **452,** 829 (2008).

[14] A. Kumar, G. A. Csáthy, M. J. Manfra, L. N. Pfeiffer, and K. W. West, *Nonconventional Odd-Denominator Fractional Quantum Hall States in the Second Landau Level*, Phys. Rev. Lett. **105,** 246808 (2010).

[15] J. Nuebler, V. Umansky, R. Morf, M. Heiblum, K. von Klitzing, and J. Smet, *Density Dependence of the $\nu = \frac{5}{2}$ Energy Gap: Experiment and Theory*, Phys. Rev. B **81,** 035316 (2010).

[16] W. Pan, N. Masuhara, N. S. Sullivan, K. W. Baldwin, K. W. West, L. N. Pfeiffer, and D. C. Tsui, *Impact of Disorder on the 5/2 Fractional Quantum Hall State*, Phys. Rev. Lett. **106,** 206806 (2011).

[17] Y. Liu, D. Kamburov, M. Shayegan, L. N. Pfeiffer, K. W. West, and K. W. Baldwin, *Anomalous Robustness of the $\nu = 5/2$ Fractional Quantum Hall State near a Sharp Phase Boundary*, Phys. Rev. Lett. **107,** 176805 (2011).

[18] J. Nuebler, B. Friess, V. Umansky, B. Rosenow, M. Heiblum, K. von Klitzing, and J. Smet, *Quantized $\nu = 5/2$ State in a Two-Subband Quantum Hall System*, Phys. Rev. Lett. **108,** 046804 (2012).

[19] Y. Liu, S. Hasdemir, M. Shayegan, L. N. Pfeiffer, K. W. West, and K. W. Baldwin, *Evidence for a $\nu = 5/2$ Fractional Quantum Hall Nematic State in Parallel Magnetic Fields*, Phys. Rev. B **88,** 035307 (2013).

[20] G. Gamez and K. Muraki, *$\nu = 5/2$ Fractional Quantum Hall State in Low-Mobility Electron Systems: Different Roles of Disorder*, Phys. Rev. B **88,** 075308 (2013).

[21] W. Pan, A. Serafin, J. S. Xia, L. Yin, N. S. Sullivan, K. W. Baldwin, K. W. West, L. N. Pfeiffer, and D. C. Tsui, *Competing Quantum Hall Phases in the Second Landau*

Level in the Low-Density Limit, Phys. Rev. B **89**, 241302 (2014).

[22] N. Deng, G. C. Gardner, S. Mondal, E. Kleinbaum, M. J. Manfra, and G. A. Csáthy, $\nu = 5/2$ *Fractional Quantum Hall State in the Presence of Alloy Disorder,* Phys. Rev. Lett. **112**, 116804 (2014).

[23] C. Reichl, J. Chen, S. Baer, C. Rossler, T. Ihn, K. Ensslin, W. Dietsche, and W. Wegscheider, *Increasing the* $\nu = 5/2$ *Gap Energy: An Analysis of MBE Growth Parameters,* New J. Phys. **16**, 023014 (2014).

[24] L. Tiemann, G. Gamez, N. Kumada, and K. Muraki, *Unraveling the Spin Polarization of the* $\nu = 5/2$ *Fractional Quantum Hall State,* Science **335**, 828 (2012).

[25] R. L. Willett, L. N. Pfeiffer, and K. W. West, *Measurement of Filling Factor 5/2 Quasiparticle Interference with Observation of Charge* $e/4$ *and* $e/2$ *Period Oscillations,* Proc. Natl. Acad. Sci. U.S.A. **106**, 8853 (2009).

[26] V. Venkatachalam, A. Yacoby, L. Pfeiffer, and K. West, *Local Charge of the* $\nu = 5/2$ *Fractional Quantum Hall State,* Nature (London) **469**, 185 (2011).

[27] M. Stern, P. Plochocka, V. Umansky, D. K. Maude, M. Potemski, and I. Bar-Joseph, *Optical Probing of the Spin Polarization of the* $\nu = 5/2$ *Quantum Hall State,* Phys. Rev. Lett. **105**, 096801 (2010).

[28] T. D. Rhone, J. Yan, Y. Gallais, A. Pinczuk, L. Pfeiffer, and K. West, *Striking Roles for Spin Degrees of Freedom in the Second Landau Level* (unpublished).

[29] C. Nayak and F. Wilczek, $2n$-*Quasihole States Realize* 2^{n-1}-*Dimensional Spinor Braiding Statistics in Paired Quantum Hall States,* Nucl. Phys. **B479**, 529 (1996).

[30] N. Read and E. Rezayi, *Quasiholes and Fermionic Zero Modes of Paired Fractional Quantum Hall States: The Mechanism for Non-Abelian Statistics,* Phys. Rev. B **54**, 16864 (1996).

[31] Y. Tserkovnyak and S. H. Simon, *Monte Carlo Evaluation of Non-Abelian Statistics,* Phys. Rev. Lett. **90**, 016802 (2003).

[32] A. Seidel, *Pfaffian Statistics through Adiabatic Transport in the 1D Coherent State Representation,* Phys. Rev. Lett. **101**, 196802 (2008).

[33] N. Read, *Non-Abelian Adiabatic Statistics and Hall Viscosity in Quantum Hall States and* $p_x + i p_y$ *Paired Superfluids,* Phys. Rev. B **79**, 045308 (2009).

[34] M. Baraban, G. Zikos, N. Bonesteel, and S. H. Simon, *Numerical Analysis of Quasiholes of the Moore-Read Wave Function,* Phys. Rev. Lett. **103**, 076801 (2009).

[35] E. Prodan and F. D. M. Haldane, *Mapping the Braiding Properties of the Moore-Read State,* Phys. Rev. B **80**, 115121 (2009).

[36] P. Bonderson, V. Gurarie, and C. Nayak, *Plasma Analogy and Non-Abelian Statistics for Ising-Type Quantum Hall States,* Phys. Rev. B **83**, 075303 (2011).

[37] R. L. Willett, L. N. Pfeiffer, and K. W. West, *Alternation and Interchange of* $e/4$ *and* $e/2$ *Period Interference Oscillations Consistent with Filling Factor 5/2 Non-Abelian Quasiparticles,* Phys. Rev. B **82**, 205301 (2010).

[38] R. L. Willett, L. N. Pfeiffer, K. W. West, and M. Manfra, *Aharonov-Bohm Effect and Coherence Length of Charge* $e/4$ *Quasiparticles at 5/2 Filling Factor Measured in*

Multiple Small Fabry-Perot Interferometers, arXiv: 1301.2594.

[39] R. L. Willett, C. Nayak, K. Shtengel, L. N. Pfeiffer, and K. W. West, *Magnetic-Field-Tuned Aharonov-Bohm Oscillations and Evidence for Non-Abelian Anyons at* $\nu = 5/2$, Phys. Rev. Lett. **111**, 186401 (2013).

[40] S. Baer, C. Rossler, T. Ihn, K. Ensslin, C. Reichl, and W. Wegscheider, *Experimental Probe of Topological Orders and Edge Excitations in the Second Landau Level,* Phys. Rev. B **90**, 075403 (2014).

[41] X. Lin, C. Dillard, M. A. Kastner, L. N. Pfeiffer, and K. W. West, *Measurements of Quasiparticle Tunneling in the* $\nu = 5/2$ *Fractional Quantum Hall State,* Phys. Rev. B **85**, 165321 (2012).

[42] R. H. Morf, *Transition from Quantum Hall to Compressible States in the Second Landau Level: New Light on the* $\nu = 5/2$ *Enigma,* Phys. Rev. Lett. **80**, 1505 (1998).

[43] E. H. Rezayi and F. D. M. Haldane, *Incompressible Paired Hall State, Stripe Order, and the Composite Fermion Liquid Phase in Half-Filled Landau Levels,* Phys. Rev. Lett. **84**, 4685 (2000).

[44] M. R. Peterson, Th. Jolicoeur, and S. D. Sarma, *Finite-Layer Thickness Stabilizes the Pfaffian State for the 5/2 Fractional Quantum Hall Effect: Wave Function Overlap and Topological Degeneracy,* Phys. Rev. Lett. **101**, 016807 (2008).

[45] M. R. Peterson, Th. Jolicoeur, and S. D. Sarma, *Orbital Landau Level Dependence of the Fractional Quantum Hall Effect in Quasi-Two-Dimensional Electron Layers: Finite-Thickness Effects,* Phys. Rev. B **78**, 155308 (2008).

[46] M. R. Peterson, *The Fractional Quantum Hall Effect at Filling Factor 5/2: Numerically Searching for Non-Abelian Anyons,* J. Phys. Conf. Ser. **402**, 012021 (2012).

[47] E. H. Rezayi and S. H. Simon, *Breaking of Particle-Hole Symmetry by Landau Level Mixing in the* $\nu = 5/2$ *Quantized Hall State,* Phys. Rev. Lett. **106**, 116801 (2011).

[48] A. Wójs, C. Toke, and J. K. Jain, *Landau-Level Mixing and the Emergence of Pfaffian Excitations for the 5/2 Fractional Quantum Hall Effect,* Phys. Rev. Lett. **105**, 096802 (2010).

[49] M. Storni, R. H. Morf, and S. D. Sarma, *Fractional Quantum Hall State at* $\nu = \frac{5}{2}$ *and the Moore-Read Pfaffian,* Phys. Rev. Lett. **104**, 076803 (2010).

[50] A. E. Feiguin, E. Rezayi, C. Nayak, and S. D. Sarma, *Density Matrix Renormalization Group Study of Incompressible Fractional Quantum Hall States,* Phys. Rev. Lett. **100**, 166803 (2008).

[51] A. E. Feiguin, E. Rezayi, K. Yang, C. Nayak, and S. D. Sarma, *Spin Polarization of the* $\nu = 5/2$ *Quantum Hall State,* Phys. Rev. B **79**, 115322 (2009).

[52] G. Moore and N. Read, *Nonabelions in the Fractional Quantum Hall Effect,* Nucl. Phys. **B360**, 362 (1991).

[53] S.-S. Lee, S. Ryu, C. Nayak, and M. P. A. Fisher, *Particle-Hole Symmetry and the* $\nu = \frac{5}{2}$ *Quantum Hall State,* Phys. Rev. Lett. **99**, 236807 (2007).

[54] M. Levin, B. I. Halperin, and B. Rosenow, *Particle-Hole Symmetry and the Pfaffian State,* Phys. Rev. Lett. **99**, 236806 (2007).

[55] M. R. Peterson, K. Park, and S. D. Sarma, *Spontaneous Particle-Hole Symmetry Breaking in the* $\nu = 5/2$ *Fractional*

Quantum Hall Effect, Phys. Rev. Lett. **101**, 156803 (2008).

[56] H. Wang, D. N. Sheng, and F. D. M. Haldane, *Particle-Hole Symmetry Breaking and the $\nu = 5/2$ Fractional Quantum Hall Effect*, Phys. Rev. B **80**, 241311 (2009).

[57] W. Bishara and C. Nayak, *Effect of Landau Level Mixing on the Effective Interaction between Electrons in the Fractional Quantum Hall Regime*, Phys. Rev. B **80**, 121302 (2009).

[58] X. G. Wen and Q. Niu, *Ground-State Degeneracy of the Fractional Quantum Hall States in the Presence of a Random Potential and on High-Genus Riemann Surfaces*, Phys. Rev. B **41**, 9377 (1990).

[59] M. R. Peterson and C. Nayak, *More Realistic Hamiltonians for the Fractional Quantum Hall Regime in GaAs and Graphene*, Phys. Rev. B **87**, 245129 (2013).

[60] I. Sodemann and A. H. MacDonald, *Landau Level Mixing and the Fractional Quantum Hall Effect*, Phys. Rev. B **87**, 245425 (2013).

[61] S. H. Simon and E. H. Rezayi, *Landau Level Mixing in the Perturbative Limit*, Phys. Rev. B **87**, 155426 (2013).

[62] R. E. Wooten, J. H. Macek, and J. J. Quinn, *Including Landau Level Mixing in Numerical Studies of the Quantum Hall Effect*, Phys. Rev. B **88**, 155421 (2013).

[63] N. Read and D. Green, *Paired States of Fermions in Two Dimensions with Breaking of Parity and Time-Reversal Symmetries and the Fractional Quantum Hall Effect*, Phys. Rev. B **61**, 10267 (2000).

[64] Z. Papić, F. D. M. Haldane, and E. H. Rezayi, *Quantum Phase Transitions and the $\nu = 5/2$ Fractional Hall State in Wide Quantum Wells*, Phys. Rev. Lett. **109**, 266806 (2012).

[65] M. P. Zaletel, R. S. K. Mong, F. Pollmann, and E. H. Rezayi, *Infinite Density Matrix Renormalization Group for Multicomponent Quantum Hall Systems*, Phys. Rev. B **91**, 045115 (2015).

[66] F. D. M. Haldane, *Fractional Quantization of the Hall Effect: A Hierarchy of Incompressible Quantum Fluid States*, Phys. Rev. Lett. **51**, 605 (1983).

[67] S. H. Simon, E. H. Rezayi, and N. R. Cooper, *Pseudopotentials for Multiparticle Interactions in the Quantum Hall Regime*, Phys. Rev. B **75**, 195306 (2007).

[68] More generally, at kth order in κ, $(k + 2)$-body interactions are generated.

[69] See Supplemental Material at http://link.aps.org/supplemental/10.1103/PhysRevX.5.021004 for the precise values used (that have two more precision digits compared to Ref. [59]).

[70] J. K. Jain, *Composite Fermions* (Cambridge University Press, Cambridge, England, 2007).

[71] M. A. Levin and X.-G. Wen, *Detecting Topological Order in a Ground State Wave Function*, Phys. Rev. Lett. **96**, 110405 (2006).

[72] A. Yu. Kitaev and J. Preskill, *Topological Entanglement Entropy*, Phys. Rev. Lett. **96**, 110404 (2006).

[73] M. Haque, O. Zozulya, and K. Schoutens, *Entanglement Entropy in Fermionic Laughlin States*, Phys. Rev. Lett. **98**, 060401 (2007).

[74] O. S. Zozulya, M. Haque, K. Schoutens, and E. H. Rezayi, *Bipartite Entanglement Entropy in Fractional Quantum Hall States*, Phys. Rev. B **76**, 125310 (2007).

[75] J. Biddle, M. R. Peterson, and S. D. Sarma, *Entanglement Measures for Quasi-Two-Dimensional Fractional Quantum Hall States*, Phys. Rev. B **84**, 125141 (2011).

[76] H. Li and F. D. M. Haldane, *Entanglement Spectrum as a Generalization of Entanglement Entropy: Identification of Topological Order in Non-Abelian Fractional Quantum Hall Effect States*, Phys. Rev. Lett. **101**, 010504 (2008).

[77] R. H. Morf, N. d'Ambrumenil, and S. D. Sarma, *Excitation Gaps in Fractional Quantum Hall States: An Exact Diagonalization Study*, Phys. Rev. B **66**, 075408 (2002).

[78] M. Storni and R. H. Morf, *Localized Quasiholes and the Majorana Fermion in Fractional Quantum Hall State at $\nu = \frac{5}{2}$ via Direct Diagonalization*, Phys. Rev. B **83**, 195306 (2011).

[79] V. Melik-Alaverdian and N. E. Bonesteel, *Composite Fermions and Landau-Level Mixing in the Fractional Quantum Hall Effect*, Phys. Rev. B **52**, R17032 (1995).

[80] V. W. Scarola, K. Park, and J. K. Jain, *Rotons of Composite Fermions: Comparison between Theory and Experiment*, Phys. Rev. B **61**, 13064 (2000).

[81] N. Samkharadze, J. D. Watson, G. Gardner, M. J. Manfra, L. N. Pfeiffer, K. W. West, and G. A. Csathy, *Quantitative Analysis of the Disorder Broadening and the Intrinsic Gap for the $\nu = 5/2$ Fractional Quantum Hall State*, Phys. Rev. B **84**, 121305 (2011).

[82] R. Morf and N. d'Ambrumenil, *Disorder in Fractional Quantum Hall States and the Gap at $\nu = 5/2$*, Phys. Rev. B **68**, 113309 (2003).

[83] L. Amico, R. Fazio, A. Osterloh, and V. Vedral, *Entanglement in Many-Body Systems*, Rev. Mod. Phys. **80**, 517 (2008).

[84] A. Bid, N. Ofek, H. Inoue, M. Heiblum, C. L. Kane, V. Umansky, and D. Mahalu, *Observation of Neutral Modes in the Fractional Quantum Hall Regime*, Nature (London) **466**, 585 (2010).

[85] M. Stern, B. A. Piot, Y. Vardi, V. Umansky, P. Plochocka, D. K. Maude, and I. Bar-Joseph, *NMR Probing of the Spin Polarization of the $\nu = 5/2$ Quantum Hall State*, Phys. Rev. Lett. **108**, 066810 (2012).